water

MDPI

Article

The Pantanal under Siege—On the Origin, Dynamics and Forecast of the Megadrought Severely Affecting the Largest Wetland in the World

Dirk Thielen [1,*], Paolo Ramoni-Perazzi [2,3], Mary L. Puche [1], Marco Márquez [1], José Israel Quintero [1], Wilmer Rojas [1], Alejandra Soto-Werschitz [3], Kai Thielen [4], Ana Nunes [5] and Renata Libonati [5,6]

1 Laboratory of Landscape Ecology and Climate, Venezuelan Institute for Scientific Research—IVIC, Caracas 1020-A, Venezuela; maryluzpuche@gmail.com (M.L.P.); marcomarquez01@gmail.com (M.M.); jisrraelquintero@gmail.com (J.I.Q.); werg05@gmail.com (W.R.)
2 Simulation and Modelling Center (CeSiMo), University of Los Andes, Mérida 5101, Venezuela; rpaolo1967@gmail.com
3 Departamento de Ecologia e Conservação, Instituto de Ciências Naturais, Universidade Federal de Lavras, Lavras 37200-900, MG, Brazil; alewerschitz@gmail.com
4 Faculty of the Environment and Natural Sciences, Brandenburg University of Technology Cottbus-Senftenberg, 03046 Cottbus, Germany; kthielen93@gmail.com
5 Departamento de Meteorologia, Universidade Federal do Rio de Janeiro, Rio de Janeiro 21941-916, MG, Brazil; ana.nunes@igeo.ufrj.br (A.N.); renata.libonati@igeo.ufrj.br (R.L.)
6 Instituto Dom Luiz (IDL), Faculdade de Ciências, Universidade de Lisboa, 1749-016 Lisboa, Portugal
* Correspondence: dirkthielen@gmail.com

Abstract: The Pantanal is the largest wetland of the world and one of the most important biodiversity hotspots in South America. An unprecedented ongoing megadrought is severely affecting its ecological functioning, flood pulse dynamics, and fire regime. Regarding this problematic, the present study generates reliable information about the following key issues: 1—Evolution and dynamics, 2—Origin and determinants, and 3—Forecast based on identified determinants and current trends. Results show that the evolution of the megadrought has been differentiable in both, space and time. As for its origin and determinants, Climate Change was ratified as one of the most important threats to the Pantanal, and to vast areas of South America, since a strong correlation was identified between megadrought's dynamics and the occurrence of intense marine heatwaves at Northern Hemisphere oceanic waters, and more specifically, at the Northeast Pacific. Results also show that the megadrought is expected to continue at both the Pantanal and the surrounding Highlands, at least until December 2023. Thus, an intensification of fires risk, extending now to areas historically flooded or perhumid should be expected, concomitantly to a very negative impact on non-fire-resistant vegetation cover, as well as ecosystem functioning and biodiversity, perhaps even worse than those from 2020, widely covered by the international media.

Keywords: megadrought; precipitation; extreme climate event; Pantanal; wetland; Brazil; sea surface temperature (SST); marine heatwave (MHW); CHIRPS V2.0; ERSSTv5

check for updates

Citation: Thielen, D.; Ramoni-Perazzi, P.; Puche, M.L.; Márquez, M.; Quintero, J.I.; Rojas, W.; Soto-Werschitz, A.; Thielen, K.; Nunes, A.; Libonati, R. The Pantanal under Siege—On the Origin, Dynamics and Forecast of the Megadrought Severely Affecting the Largest Wetland in the World. *Water* **2021**, *13*, 3034. https://doi.org/10.3390/w13213034

Academic Editor: Momcilo Markus

Received: 21 August 2021
Accepted: 15 October 2021
Published: 29 October 2021

Publisher's Note: MDPI stays neutral with regard to jurisdictional claims in published maps and institutional affiliations.

Copyright: © 2021 by the authors. Licensee MDPI, Basel, Switzerland. This article is an open access article distributed under the terms and conditions of the Creative Commons Attribution (CC BY) license (https://creativecommons.org/licenses/by/4.0/).

1. Introduction

The Pantanal is the largest wetland in the world [1–3]. It was designated a World Heritage Site by UNESCO in 2000. Besides a high number of resident animal species, the Pantanal is also very important biome for the migratory ones, making this wetland one of the most important biodiversity hotspot in South America [4,5]. The Pantanal functions as a large reservoir that collects water from the surrounding Highlands during the rainy season and then gradually delivers it to the lower sections of the Paraguay River resulting in characteristic and historically predictable seasonal flooding or flood pulse [6,7]. Here, human activities mostly rely on ecosystem services, and include cattle farming, agriculture,

professional and recreational fishing, and contemplative ecotourism [8]. Due to Pantanal's strong dependence on hydrological factors, changes in temperature and precipitation resulting from climatic change [9,10] may profoundly alter ecosystem functions.

Now, along with expanding agricultural activities and hydroelectric development, climate change poses a major threat to the Pantanal [11,12]. Regarding the climate change problematic, Thielen et al. [13] forecasted extended periods of severe drought for the Pantanal and surrounding areas as an immediate response to the current warming trend in the Sea Surface Temperature (SST) in specific oceanic regions of Northern Hemisphere, mainly from Northeast Pacific.

SST is a key variable in the climate system regulating thermal and dynamical interactions between the ocean and atmosphere. Compared to most other ocean variables, SST is well sampled over the open ocean, especially since satellite measurements became available in 1979 [14]. The study of the effects of anomalously warm SST began little after, in the early 1980s, when research into the ENSO phenomenon intensified, mainly due to the occurrence of the mega-Niño 1982/1983 [15]. After this event, researchers began noticing that warm water events were becoming more frequent, but it was not until 2018 that this was demonstrated with global observations [16].

Marine heatwaves (MHWs) are anomalously warm water events that may last many months and extend over thousands of square kilometers [17], capable of generating severe impacts on natural systems functioning, as well as in the socioeconomic ones. Several prominent MHWs have attracted scientific and public interest, and recent assessments have documented global and regional increases in their frequency and intensity, and regardless of the physical mechanisms driving individual MHWs, consensus is emerging that anthropogenic climate change has significantly increased the likelihood of recent MHWs [18].

Now, few months after the publication of Thielen et al. [13] forecast, the effects of a developing severe drought in the largest wetland in the world started to be of mayor concern, not only by locals, but by the international community. According to the Marinha do Brasil [19], the Paraguay River at Ladário has maintained a deficient water level of about 48% for June 2020 and near 62% for June 2021 (series 2016–2020), and June is precisely the month that usually marks the peak of the river throughout the year [20]. According to Libonati et al. [21], by December 2020 the ongoing drought was already considered to be the most prolonged and most severe in the last 60 years, and induced a wet season 2019–2020 with 60% less rain than normal [20].

Droughts are ranked the highest among all-natural hazards, causing substantial damages to humans, the environment, and the economy [22]. As a result, the 2020's fires in the Pantanal were unprecedented in extent and duration: about 40,000 km^2 of the area of this important wetland went up in flames that year [23], from which 43% of the area had not been burnt previously in the last two decades [24]. Such fire outbreak was the result of a complex interplay among meteorological/climatic, landscape, and human factors [24,25]. Where, most certainly, a prevailing extreme dry condition, generated by the ongoing megadrought, represents an important determinant [26]. Due to its wetter condition, fires in the Pantanal are much less frequent and spatially restricted than in the drained savannas from the neighboring Cerrado [23]. Any case, the 2020's fires destroyed infrastructure, including cattle ranches and bridges. Jaguars (*Panthera onca*), hyacinth macaws (*Anodorhynchus hyacinthinus*), and other iconic wildlife were directly affected (died, suffered severe injuries, or starved), along with countless resident and migratory species [24]. It is not possible to have an exact number of animals affected, still, based on known species densities, Berlinck et al. [27] estimate this number in at least 65 million native vertebrates. International media such as Reuters (30 August 2020), Deutsche Welle (2 August 2020), Vox (17 September 2020), Euronews (10 October 2020), New York Times (13 October 2020), Bloomberg (31 October 2020), Al Jazeera (12 October 2020), CNN (13 November 2020), repeatedly made coverage of such unprecedented event.

Although wide reference was achieved about the direct effects on environmental and societal issues, besides that provided by Thielen et al. [13], little evidence was available, to the media, to stakeholders and to policy-makers, regarding key issues such as the dynamics, origin, and forecast of the extreme drought that already is considered to be the most prolonged and most severe in the last 60 years [21], and that has already severely affected the Pantanal [20]. Which, as forecasted by Thielen et al. [13], and according to preliminary observations from Thielen et al. [26], may be part of an ongoing global extreme oceanic event (i.e., an extreme MHW) generating an unprecedented climatic response (i.e., a megadrought) that might be far from over.

Thus, the main objective of this work was to generate reliable information about three key issues regarding the megadrought severely affecting the largest wetland in the world. First, to characterize its spatial and temporal dynamics along the different regions and subregions from the Pantanal and surrounding areas, and since its very beginning until present. Second, to evaluate recent oceanic SST dynamics and identify the oceanic region that best explains current megadrought in terms of its duration and intensity. And third, to generate a reliable forecast based on identified determinants and current trends. The combined use of remote sensed data from different sources, analyzed through sophisticated spatial analysis tools, allowed this study to generate reliable information about the evolution of current megadrought has been differentiable in both, space and time. An evolution that was not explained by the SST dynamics from neighboring oceanic regions, but rather from much far distanced regions such as the Northeast Pacific. From which, the presence of a very intense and prolonged warm SST gives solid hints to expect as to forecast for the megadrought to last much longer and to be even more pervasive.

2. Materials and Methods

2.1. Study Area

The study area consisted of regions and sub-regions of the Upper Paraguay River Basin (UPRB) which forms part of the upper La Plata River Basin [28] within west-central Brazil. With a total extension of 361,338 km^2, it includes the Pantanal (138,183 km^2), a run-on drainage area occupying the center of the UPRB, and the Highlands (223,155 km^2, see Figure 1), which consists of the surrounding watershed areas at (or above) elevations of 200 m asl.

According to Silva and Abdon [29], the Pantanal can be further divided into 11 sub-regions: Porto Murtinho (P-01; 3839 km^2), Nabileque (P-02; 13,281 km^2), Miranda (P-03; 4383 km^2), Aquidauana (P-04; 5008 km^2), Abobral (P-05; 2833 km^2), Nhecolândia (P-06; 26,921 km^2), Paiaguás (P-07; 27,082 km^2), Paraguai (P-08; 8147 km^2), Barão de Melgaço (P-09; 18,167 km^2), Poconé (P-10; 16,066 km^2), and Cáceres (P-11; 12,456 km^2). As for the surrounding Highlands, the subdivision of seven sub-regions connected to each Pantanal sub-region, identified by Thielen et al. [13], was used. These sub-regions include the H-01/02 (24,461 km^2) watershed of the Porto Murtinho and Nabileque areas, the H-03 (19,708 km^2) watershed of the Miranda area, the H-04 (22,371 km^2) watershed of the Aquidauana area, the H-06/07 (31,530 km^2) watershed of the Nhecolândia and Paiaguás areas, the H-09 (38,210 km^2) watershed of the Barão de Melgaço area, the H-10 (35,600 km^2) watershed of the Poconé area, and the H-11 (51,275 km^2) watershed of the Cáceres area. A characterization of each of aforementioned regions and subregions is provided in Table 1.

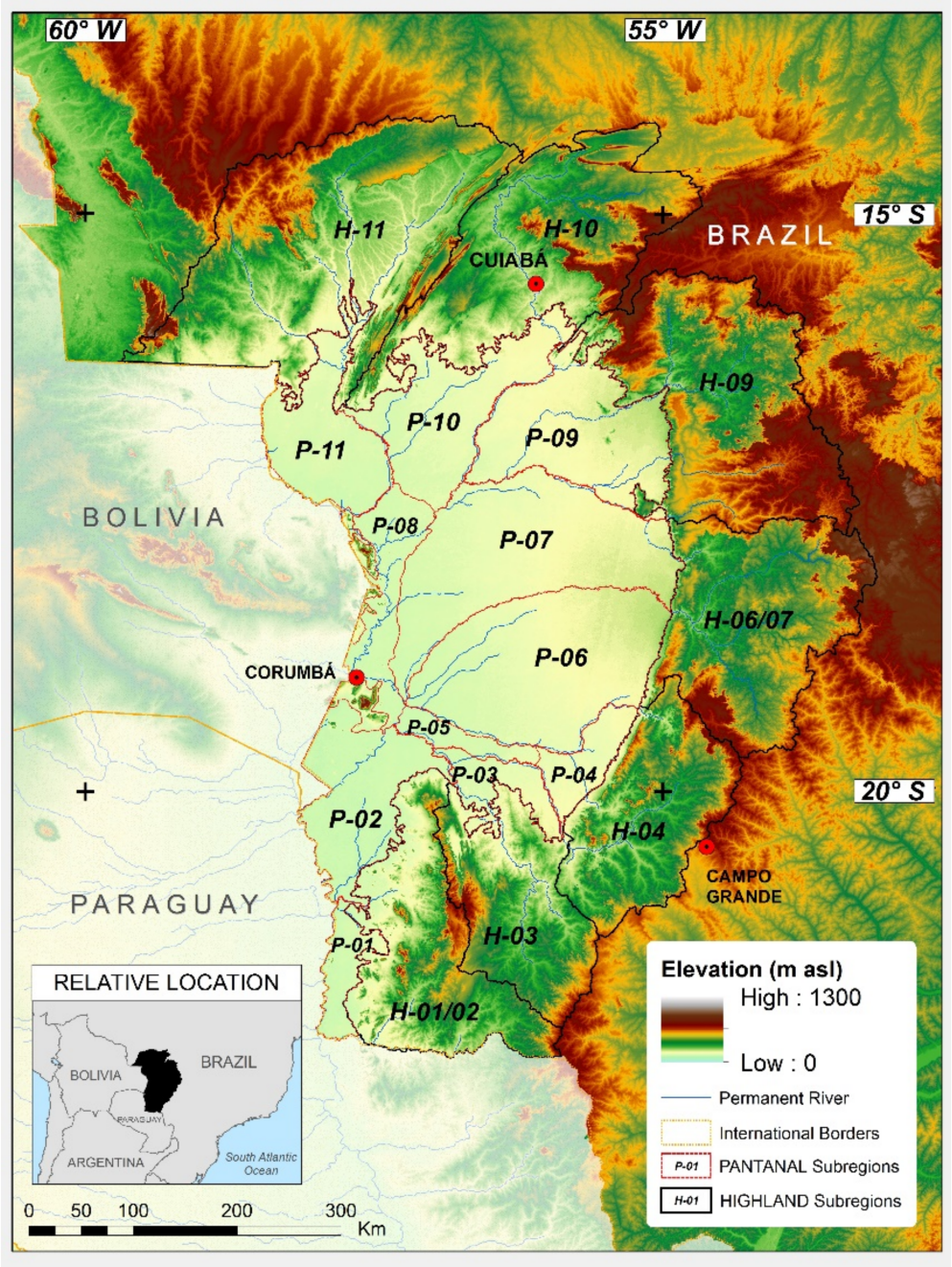


Figure 1. Map of the study area of the Upper Paraguay River Basin (UPRB) encompassing the Pantanal and the surrounding Highlands. Pantanal sub-regions are: Porto Murtinho (P-01), Nabileque (P-02), Miranda (P-03), Aquidauana (P-04), Abobral (P-05), Nhecolândia (P-06), Paiaguás (P-07), Paraguai (P-08), Barão de Melgaço (P-09), Poconé (P-10) and Cáceres (P-11), and were taken from Silva and Abdon [29]; while Highland sub-regions (H-01/02, H-03, H-04, H-06/07, H-09, H-10 and H-11), draining to the different Pantanal sub-regions, were adapted from Thielen et al. [13].

Table 1. Characteristics of the regions and subregions encompassed in the study area regarding several physical, natural and anthropic variables. In each case, the values were estimated by means of GIS tools and from freely available sources.

	Size [1] (in km^2)	Mean [2] Altitude (m asl)	Population Density by 2018 [3] (Hab/Ha)	Land Use and Land Cover by 2014 [4] (in % of the Area)										Permanent River Streams [5] (in km)
				Anthropic Use	Natural Cover	Forest Formation	Woodland Savanna	Shrubby Savanna (Cerrado)	Grassland Savanna	Alteration/ Natural Management	Steppe-Type Savanna/ Chaco wetland	Vegetation with Fluvial Influence	Permanent Surface Water	
UPRB	361,338	263	2.54	29.38	70.62	6.21	8.29	14.22	16.74	3.03	6.23	13.69	2.22	2222
HIGHLANDS	223,155	352	3.09	59.13	40.87	9.51	7.27	9.88	9.84	0.06	3.35	0.94	0.03	322
PANTANAL	138,183	119	2.18	10.45	89.55	4.12	8.94	16.98	21.13	4.92	8.06	21.79	3.62	1900
HIGH 01-02	24,461	250	2.17	52.11	47.89	9.78	5.65	4.48	3.43	0.00	23.34	1.21	0.00	2065
HIGH 03	19,708	295	2.59	67.27	32.73	11.38	5.63	8.73	4.99	0.00	0.06	1.95	0.00	1451
HIGH 04	22,371	339	2.40	63.81	36.19	7.93	4.99	8.22	15.03	0.02	0.00	0.00	0.00	2212
HIGH 06-07	31,530	425	2.32	69.27	30.73	5.27	12.04	4.06	9.36	0.00	0.00	0.00	0.00	3795
HIGH 09	38,210	482	3.77	59.99	40.01	7.47	6.20	11.38	14.30	0.13	0.00	0.52	0.00	4364
HIGH 10	35,600	332	5.25	41.72	58.28	6.81	9.06	22.07	17.23	0.19	0.02	2.90	0.01	4271
HIGH 11	51,275	300	3.15	59.77	40.23	17.91	7.32	10.20	4.53	0.06	0.00	0.03	0.16	5340
P-01	3839	92	3.49	18.89	81.11	11.50	0.20	1.29	0.66	1.72	24.89	37.86	2.99	512
P-02	13,281	85	1.38	3.73	96.27	5.78	0.08	2.03	2.03	1.67	59.96	19.79	4.92	2080
P-03	4383	115	2.48	18.36	81.64	2.29	10.22	18.76	35.60	9.15	0.83	4.79	0.00	831
P-04	5008	129	0.70	24.16	75.84	2.34	9.55	23.54	22.58	2.24	0.00	15.59	0.00	688
P-05	2833	97	0.83	0.59	99.41	0.08	15.96	0.01	64.64	2.01	0.44	2.10	14.17	769
P-06	26,921	129	0.56	9.21	90.79	0.92	17.01	21.91	25.01	6.66	0.00	19.24	0.04	2277
P-07	27,082	127	0.91	9.12	90.88	3.83	9.85	31.12	22.94	8.51	0.00	12.90	1.73	3538
P-08	8147	94	6.23	4.56	95.44	8.68	5.62	0.11	13.67	0.00	2.51	51.73	13.11	1581
P-09	18,167	145	1.70	14.42	85.58	7.35	8.13	49.62	4.63	3.06	0.00	12.81	0.00	2695
P-10	16,066	118	1.20	7.66	92.34	2.10	17.15	21.47	18.48	8.76	0.00	23.34	1.05	2530
P-11	12,456	106	4.52	4.21	95.79	0.40	4.61	16.94	22.17	10.30	0.00	39.55	1.82	1143

[1] Thielen et al. [13]; [2] Freely available at https://www2.jpl.nasa.gov/srtm/southAmerica.htm (accessed on 10 October 2021); [3] Freely available at https://www.worldpop.org/doi/10.5258/SOTON/WP00674 (accessed on 10 October 2021); [4] Freely available at https://www.embrapa.br/pantanal/bacia-do-alto-paraguai (accessed on 10 October 2021); [5] Freely available at https://www.diva-gis.org/gdata (accessed on 10 October 2021).

2.2. Data

Precipitation data was obtained from the Climate Hazards group Infrared Precipitation with Stations (CHIRPS), freely available at https://iridl.ldeo.columbia.edu/SOURCES/.UCSB/.CHIRPS/.v2p0/.monthly/.global/ (accessed on 10 October 2021). CHIRPS V2.0 is a quasi-global gridded rainfall time series dataset, spanning 50° S–50° N, from 1981 to near-present, 0.05° resolution satellite imagery with in situ station data [30], with great applications monitoring precipitation extremes [13,26]. According to Beck et al. [31], in a global-scale evaluation of 23 precipitation datasets, CHIRPS V2.0 tends to perform the best in hydrological modeling of tropical regions, specifically in Central America, and in central and eastern Brazil. Thielen et al. [13], as well as Marengo et al. [20], tested its applicability and potentiality in the study of precipitation spatial-temporal dynamics at the UPRB. For the present study, monthly data for the time series January 1981/June 2021 was obtained from 486 rasters. Monthly and annual means, as well as some other basic precipitation parameters, were obtained by using GIS applications.

Quantifying global trends and variability in SST is of fundamental importance to understanding changes in the Earth's climate. One approach to observing SST is via remote sensing [32]. In this sense, the monthly mean SST remote sensed data was provided by the NOAA Extended Reconstructed Sea Surface Temperature Version 5 dataset (ERSSTv5), which is a global dataset derived from the International Comprehensive Ocean-Atmosphere Dataset (ICOADS). It is produced on a 2 × 2-degree grid with spatial completeness enhanced using statistical methods (http://iridl.ldeo.columbia.edu/maproom/Global/Ocean_Temp/Monthly_Temp.html, (accessed on 10 October 2021)). For the present study, monthly data for the time series January 1982/June 2021 was obtained from 474 rasters.

2.3. Calculation of the Standardized Pluviometric Drought Index—SPDI

In this study, precipitation spatial-temporal dynamics was analyzed by the Standardized Pluviometric Drought Index (SPDI) developed by Pita-López [33]. The SPDI is a monthly rainfall index that is based on the calculation of cumulative monthly rainfall anomalies, similar to the well-known Standardized Precipitation Index (SPI) of McKee et al. [34], more specifically, the 12-month SPI. As in this index, values ranging from +1 to +1.5 and +1.5 to +2.0 are associated with moderately humid and very humid episodes, respectively, and values exceeding +2 are representative of extremely humid episodes. Moderately dry, very dry and extremely dry spells are characterized by the same ranges with a negative sign (see Table 2). The SPDI is calculated as follows:

First stage:

$$APi = Pi - P_{MED}, \quad (1)$$

where APi is the monthly precipitation anomaly, Pi is the monthly precipitation, and P_{MED} is the median precipitation of the month for the series. As for this study: 1981–2010.

Second stage:

$$APAi = \sum APi, \quad \text{From} i = \text{negative } AP \text{ to } i = \text{positive } AP \quad (2)$$

where $APAi$ is the accumulated precipitation anomaly of the month.

Third Stage:

$$SPDI = \left(APAi - \overline{APA}\right)/\sigma APA, \quad (3)$$

where $\overline{APA}$ is the average value of accumulated precipitation anomalies of all the months of the series, and σAPA is the standard deviation of accumulated precipitation anomalies of all the months of the series.

GIS applications allowed to implement these equations to the 486 aforementioned CHIRPS V2.0 rasters and generate SPDI products such as images of 0.05° resolution or monthly zonal values, and at different space and/or time criteria. In the present study, monthly values of SPDI were estimated based on the climatological series 1981–2010. From this information, most recent spatial-temporal precipitation anomaly dynamics regarding current megadrought was identified for the UPRB, as well as for the Pantanal and the

Highlands, and their respective sub-regions (see Figure 1). Significance of statistical difference between sets of monthly precipitation and/or SPDI values was identified by two-tailed Paired *t*-Test ($\alpha = 0.01$). While similarities in spatial-temporal dynamics of SPDI between the different sub-regions were identified by Cluster Analysis (K-means clustering using Euclidean distance). Gong and Richman [35] noted that nonhierarchical methods, such as the K-means algorithm, outperformed hierarchical methods (the Ward's method and the average linkage method) when tested with precipitation data, as well as for SPI series [36].

Table 2. Categories resulting from SPDI estimation, adapted from McKee et al. [34] and WMO [37].

SPDI Values	Category
≥2.0	Extremely wet
1.5–2.0	Severely wet
1.0–1.5	Moderately wet
−1.0–1.0	Near-normal
−1.0–−1.5	Moderate drought
−1.5–−2.0	Severe drought
≤−2.0	Extreme drought

2.4. Calculation of Sea Surface Temperature Anomalies (SSTA) and Marine Heatwave Condition

Monthly SSTA was estimated based on the climatological series January 1982/December 2011, and for the following oceanic regions: *PAC-NE*—Pacific Northeast, *PAC-NW*—Pacific Northwest and *ATL-N*—Atlantic North, at the Northern Hemisphere; and *ATL-SC*—Atlantic South Central, *ATL-S*—Atlantic South, *PAC-SAC*—Pacific South American Coast, *PAC-S*—Pacific South, and *IND-S*—Indian South, at the Southern Hemisphere (see Figure 2). According to Thielen et al. [13], these specific oceanic regions show the strongest (positive or negative) correlation with historical precipitation dynamics at the UPRB (series 1981–2018). Additionally, traditional SST indexes such as *TNA*—Tropical North Atlantic and *TSA*—Tropical South Atlantic, as well as *NEP*—Northeast Pacific, and the ENSO regions: *NIÑO 1+2*, *NIÑO 3* and *NIÑO 3.4*, described by PSL/NOAA [38] and CPC/NCEP/NOAA [39], were considered in the present study. Mann-Kendall tests were applied to determine the significance of the time series trends in the monthly SSTs for each oceanic zone.

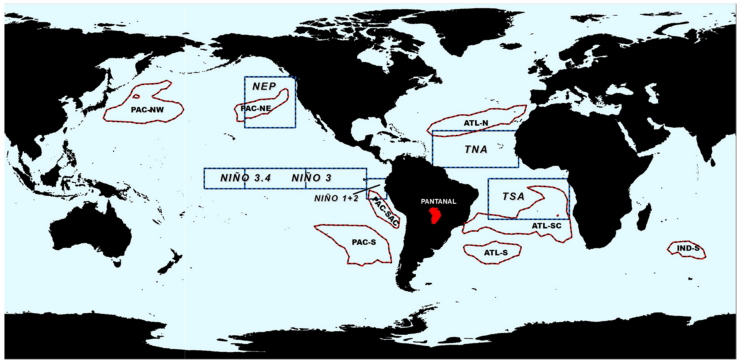


Figure 2. Oceanic regions and traditional SST indexes considered in the present study. The oceanic regions (in dashed red lines) were taken from Thielen et al. [13] and are as follows: *PAC-NE*—Pacific Northeast (2.7 M km^2), *PAC-NW*—Pacific Northwest (7.1 M km^2) and *ATL-N*—Atlantic North (5.2 M km^2), at the Northern Hemisphere; and *ATL-SC*—Atlantic South Central (9.0 M km^2), *ATL-S*—Atlantic South (3.2 M km^2), *PAC-SAC*—Pacific South American Coast (1.5 M km^2), *PAC-S*—Pacific South (6.5 M km^2), and *IND-S*—Indian South (1.6 M km^2), at the Southern Hemisphere. The traditional SST indexes (in dashed blue lines) include: *NEP*—Northeast Pacific (9.9 M km^2), *TNA*—Tropical North Atlantic (9.8 M km^2) and *TSA*—Tropical South Atlantic (10.1 M km^2); as well as the ENSO regions: *NIÑO 1+2* (1.2 M km^2), *NIÑO 3* (7.4 M km^2) and *NIÑO 3.4* (6.2 M km^2).

A Marine Heatwave (MHW), which is an anomalously warm water event that may last many months and extend over thousands of square kilometers, was identified and categorized following Hobday et al. [17]. According to these authors, the different categories of MHWs are based on multiples of the difference between the climatological mean (January 1982/December 2011) and the climatological 90th percentile, where: Moderate (1–2×, Category I), Strong (2–3×, Category II), Severe (3–4×, Category III), and Extreme (>4×, Category IV).

2.5. Calculation of Correlation of Precipitation with the Oceanic SSTs

GIS analytical tools were used to investigate correlations between mean monthly SST and mean monthly precipitation in the Pantanal and the surrounding Highlands. The application of correlation analysis permits the identification of regions where the interactions between hydrological droughts and teleconnection are strong [40]. Results from Section 2.3, that is from the precipitation spatial-temporal dynamics, were used to identify the series that best describes current megadrought. While results from Section 2.4 provided hints about the oceanic region with most significant SST variability. Analysis assumed that the observed SST preceded precipitation by lead times of 0 to 6 months. The Pearson correlation coefficient was used to estimate the degree of explained variance ($\alpha = 0.01$) between the monthly SST and precipitation. A paired, two-tailed *t*-Test was used to assess the significance of statistical differences. Confidence intervals of 99% were used to identify correlation coefficients (r) ranges. Close attention was paid to resulting correlations that would best explain recent precipitation dynamics (2019–present) at the Pantanal and the surrounding Highlands.

A scheme of the workflow for the methodology of the present research is provided in Figure 3.

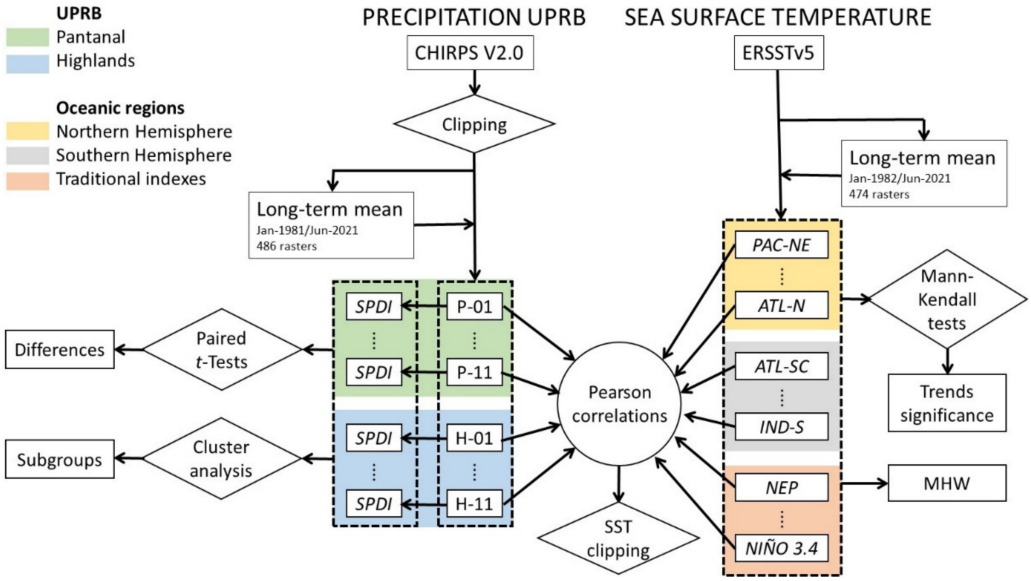


Figure 3. Scheme of the workflow, which was based on the time series from January 2019 until June 2021, except when indicated. Land and oceanic regions were described in Figures 1 and 2, respectively.

3. Results

3.1. Megadrought's Evolution

3.1.1. Temporal Dynamics

Monthly analysis of precipitation dynamics for the series January 1981–June 2021 shows that the Pantanal is significantly drier than surrounding Highlands ($p < 0.01$). Even though the Highlands showed annual precipitation amounts to be about 19% higher than in the Pantanal (1454 vs. 1176 mm/year, respectively), rainfall here was less variable: over 90% of months during this series had SPDI near-normal ($(-1.0 \leq \text{SPDI} < 1.0)$. Until the

beginning of 2020, precipitations events at the Highlands capable of generating abnormal SPDI values, either for dry or a wet condition, were rather short-lived and moderately intense (see Figure 4). Since June 2019 onwards, the monthly precipitation amounts suffered a reduction of about 30% from historical mean. Right from January 2020, precipitation anomaly in the Highlands passed from moderate drought ($-1.5 \leq$ SPDI < -1.0) to a severe drought condition ($-2.0 \leq$ SPDI < -1.5), reaching a sustained extreme drought condition (SPDI ≤ -2.0) from September 2020 onwards.

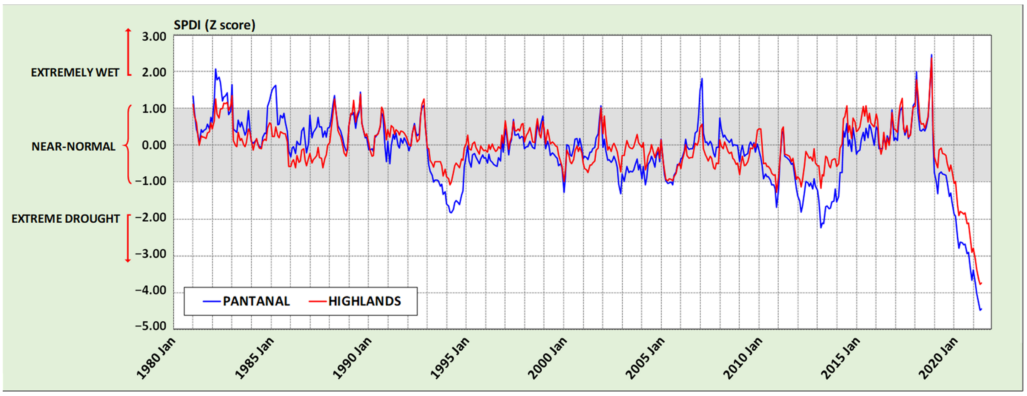


Figure 4. Temporal dynamics of precipitation anomalies for the series January 1981–June 2021 at the Pantanal and the surrounding Highlands. Precipitation anomalies are measured as Standardized Precipitation Drought Index (SPDI) and interpreted using SPI classification system from McKee et al. [34] and WMO [37] (see Table 2). The grey area represents the near-normal condition (i.e., $-1.0 \leq$ SPDI < 1.0).

As for the Pantanal, during the series January 1981–June 2021, about 78% of the months showed a near-normal precipitation condition. Here, anomalies in precipitation, dry or wet, occurred in longer pulses than in surrounding Highlands. In the Pantanal, dry spells have been significantly more frequent than wet ones ($p < 0.01$; 15.9 vs. 6.4% of the months). Three main dry spells have occurred in the Pantanal in the last 40 years (see Figure 4). The first one is a moderate drought lasting 15 months (September 1993/November 1994) with a mean SPDI value of -1.48. A second dry spell of 14 months (January 2013/February 2014) generated a severe dry anomaly in the Pantanal (mean SPDI = -1.68), and during three months (from March/May 2013), precipitation anomalies generated an extreme drought condition (SPDI ≤ -2.0). None of these two dry pulses affecting the Pantanal generated precipitation anomalies in the surrounding Highlands. As for the third dry spell, and like it had occurred in the neighboring higher lands, since June 2019 onwards, the monthly precipitation amounts at the lowlands of the Pantanal underwent an important reduction from the historical mean (of about 32%). As for resulting SPDI values, the drought condition was reached four months' sooner in the Pantanal than in the Highlands (September 2019 and January 2020, respectively). The evolution of this particular dry spell has been most dramatic in the Pantanal—in the term of only six months, the precipitation anomalies passed from a near-normal condition to a sustained extreme drought condition (SPDI ≤ -2.0).

Such evolution is also appreciated in Figure 5 which represents the temporal dynamics of the SPDI monthly values from January 2019 to June 2021, together with mean historic and observed precipitations, at the Pantanal and the surrounding Highlands. As for the Pantanal, from June 2019 onward, 83.3% of the months had precipitations below the historical values. This value was 87.5% in the case of the Highlands. Such persistent precipitation anomaly generated an extreme drought that passed to affect initially around 5.7% of the Pantanal area in June 2019, to 41.5% in January 2020 (Figure 5a). By March 2020, over 90% of the Pantanal was affected by a drought condition (SPDI < -1.0), and over 60% by an extreme drought (SPDI ≤ -2.0). The extreme drought condition not only has persisted for a long time in the Pantanal, but it has expanded very importantly: 82.2%

by June 2021. Even though the number of abnormally dry months generating the extreme and extended drought in the Pantanal was not significantly different ($p > 0.05$) from that occurred in the Highlands, here, the drought had a more discrete dynamic (Figure 5b). It is only by September 2020, six months later than in the lower lands, that 50.7% of the Highlands area was affected by the extreme drought condition. As for most recent update, June 2021, 70.5% of the Highlands was affected by a drought condition, from which 56.1% by an extreme drought.

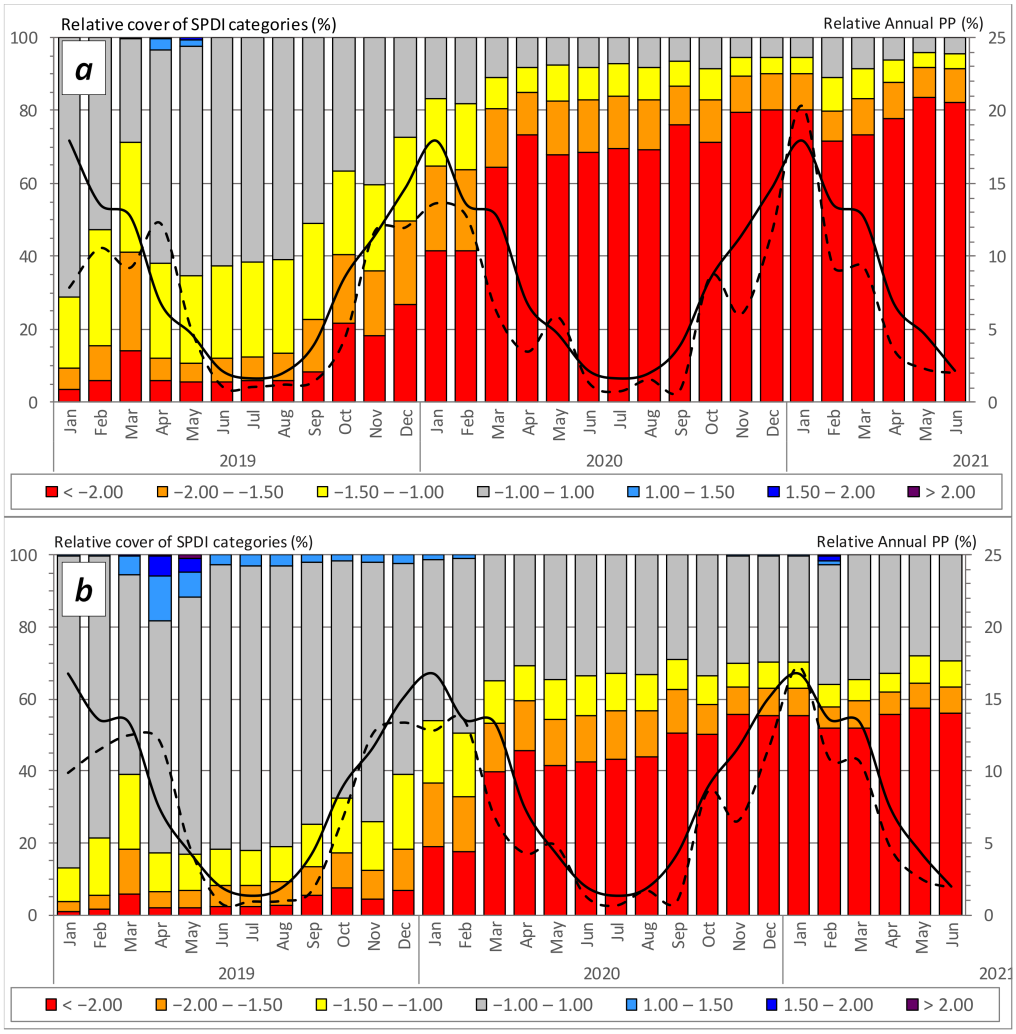


Figure 5. Relative cover (%) of SPDI categories at (**a**) the Pantanal and (**b**) the surrounding Highlands. Categories were adapted from McKee et al. [34] and WMO [37] and correspond to the following SPDI range of values: ≤−2.0, Extreme drought; −2.0–1.5, Severe drought; −1.5–−1.0 Moderate drought; −1.0–−1.0, Near-normal; 1.0–1.5, Moderately wet; 1.5–2.0, Severely wet; and ≥2.0, Extremely wet. Solid line is the historical monthly mean precipitation for the climatological series 1981–2010, while the dashed line is the observed amount precipitated. Both lines, expressed as relative to annual precipitation (in %).

3.1.2. Spatial Dynamics

Spatial dynamics of the drought (January 2019 to June 2021) in the UPRB is given in Figure 6. Here, differences between the Pantanal and the surrounding Highlands, as well as in their different sub-regions, are better observed. According to this figure, the drought dynamics along the series is spatially differentiable. First evidence of a drought developing was observed in the sub-region of Paraguai (P-08) in central section of the Pantanal, showing a severe drought right from the beginning of 2019. Along the first year,

and specifically by the second half, an easterly spread of the drought occurred. First as moderate ($-1.5 \leq$ SPDI < -1.0) and reaching the severe condition ($-2 \leq$ SPDI < -1.5) by the end of 2019. By the end of the first trimester of 2020, and from there on, the extreme drought condition (SPDI ≤ -2.0) was generalized in the middle and most of the northern section of the Pantanal and corresponding Highlands. Only the southernmost sectors of the UPRB, and a small section of the Highlands (H-11) draining to Cáceres (P-11), showed near-normal precipitations during the entire series.

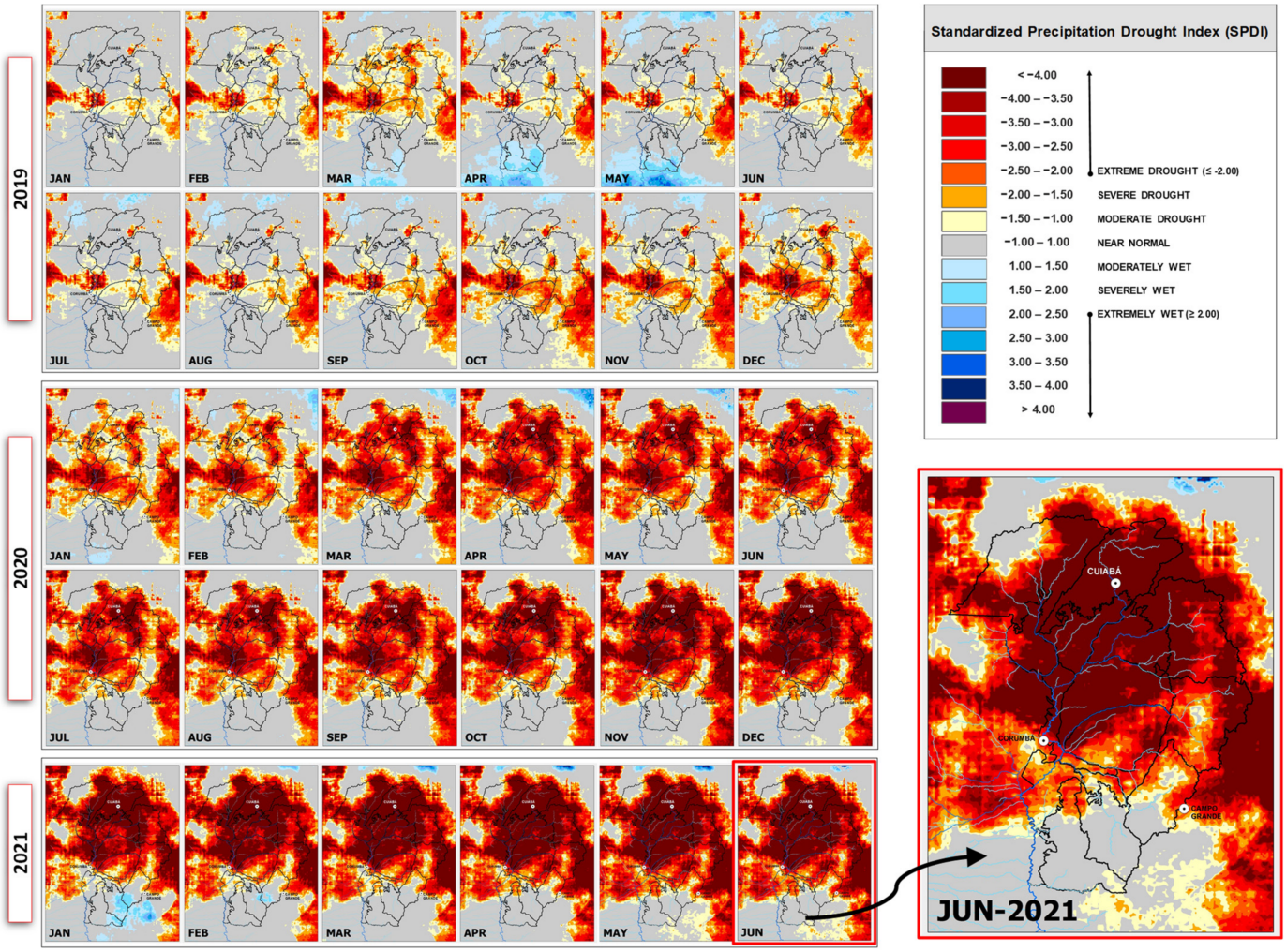


Figure 6. Spatial-temporal dynamics of the Standardized Precipitation Drought Index (SPDI) from January 2019 to June 2021 at the of the Upper Paraguay River Basin (UPRB) encompassing the Pantanal and the surrounding Highlands. Sub-regions are described in Figure 1. SPDI categories were adapted from McKee et al. [34] and WMO [37].

Accurate quantification of such dynamics is given in Figure 7. For instance, the central Pantanal sub-region of Paraguai (P-08), from the beginning of the series until October 2019 reached a mean SPDI of −1.84 (named Group 1, according to Figure 7a,b). From that moment on, precipitation anomalies generated a sustained decreased in SPDI values from −2.54 in October 2019 to −5.92 in June 2021. As for other areas in the UPRB, by the second half of 2019, a moderate drought condition (mean SPDI = −1.36) started to spread rather heterogeneously from the middle sub-regions of the Pantanal [Paiaguás (P-07), Nhecolândia (P-06), Aquidauana (P-04), Cáceres (P-11)] as well as the Highland sub-region H-06/07 (Figure 7a,b). By the beginning of 2020, four other sub-regions, two from the Pantanal [Barão de Melgaço (P-09) and Poconé (P-10)] and two from the Highlands (H-09 and H-10), were importantly affected by the spreading severe drought (mean SPDI = −1.55). For the rest of the series, the drought became increasingly extreme (mean SPDI March/October

2020 = −2.97 vs. December 2020/June 2021 = −4.56) and more homogeneous (mean relative area March/October 2020 = 79.7% vs. December 2020/June 2021 = 91.9%) in aforementioned group of nine sub-regions (Group 2, according to Figure 7a,b).

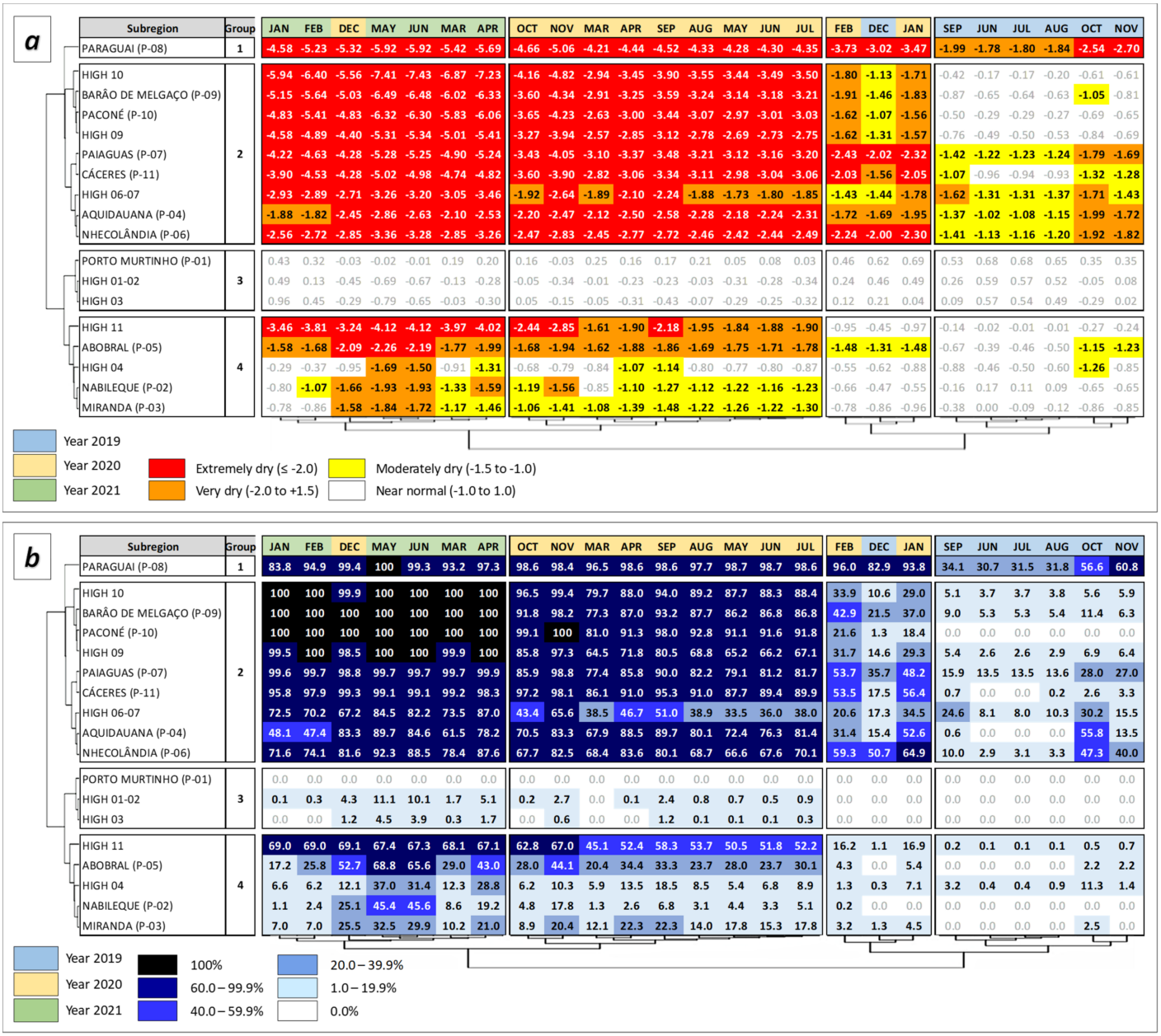


Figure 7. (**a**) Monthly mean Standardized Precipitation Drought Index (SPDI) dynamics from June 2019 to June 2021 at the different sub-regions of the Pantanal and the surrounding Highlands. (**b**) Relative area of aforementioned sub-regions with an extreme drought condition (SPDI ≤ −2.0). Sub-regions were taken from Thielen et al. [13]. Cluster analysis (K-means clustering using Euclidean distance) was performed to both rows and columns, and with the statistical tool ClustVis [41].

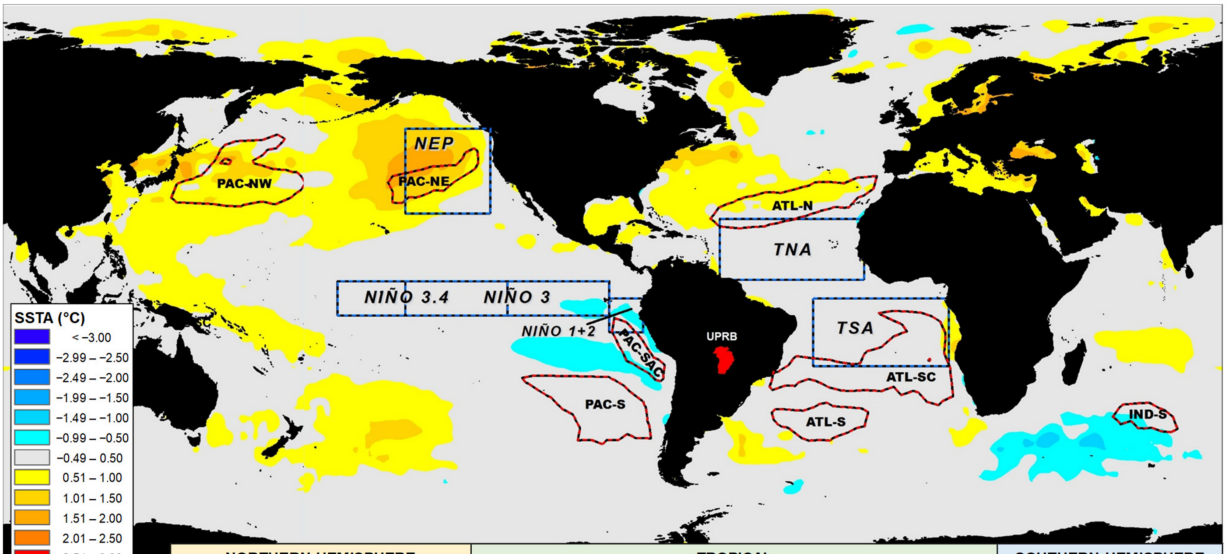
During the entire series, that is from June 2019 until June 2021, there are three sub-regions that did not show any precipitation anomaly (mean SPDI = 0.08): Porto Murtinho (P-01) in the Pantanal, and in the neighboring Highland the sub-regions of H-01-02 and H-03; all three located in the southern most section of the UPRB (Group 3, according to Figure 7a,b). There is also a fourth group of sub-regions regarding their latter and/or more spatial heterogeneous response in precipitation anomaly dynamics (Group 4, Figure 7a,b), comprising the Pantanal sub-regions of Nabileque (P-02), Miranda (P-03), and Abobral (P-05), and by the two Highland sub-regions of H-04 and H-11). Here, drought conditions did

not start until March or April 2020. Although for Abobral (P-05) and H-11, the drought was from severe to extreme for the rest of the series (mean SPDI = −1.94 and −3.82, respectively), drought conditions in the other three sub-regions were less intense (moderate) and less spread (heterogeneous), and even intermittent, as in the case of the southern highland sub-region of H-04.

3.2. Sea Surface Temperature (SST) Dynamics

3.2.1. Sea Surface Temperature Anomaly (SSTA) at the Different Oceanic Regions

Figure 8 shows the resulting mean SSTA for the series June 2019/June 2021 at the different oceanic regions and SST indexes (see Figure 2). It was established that most significant SST dynamics ($p < 0.01$) resulted from the warming of oceanic waters in the Northern Hemisphere, more specifically in the three regions already identified by Thielen et al. [13], such as: *PAC-NE*, *PAC-NW* and *ATL-N*, with resulting mean SSTA of 1.28, 0.77 and 0.50 °C, respectively. In absolute terms, resulting SSTA at *PAC-NE* was from 3–6× higher than that for any of the ENSO regions, and 6–9× higher than for any referential SST indexes such as *TNA* and *TSA*. As for *NEP*, and even tough 81% of *PAC-NE* area is comprised in this northeast oceanic region, resulting *NEP*'s mean SSTA is significantly lower than that of *PAC-NE* ($p < 0.01$; 1.04 vs. 1.28 °C, respectively). As for *PAC-NE*, during the series June 2019/June 2021, 88% of the area presented monthly mean SSTA between 1.0 and 2.0 °C, with a maximum of 2.21 °C in August 2019. While for *NEP*, anomalies of such intensities involved a lesser area: 51%, reaching a maximum of 2.02 °C also by August 2019. *PAC-NW*, on the other side, had a lesser extended and warm SST: only 23% of the area involved SSTA >1.0 °C, and 59% involved SSTA between 0.5 and 1.0 °C. On another ocean, the Atlantic, such mild warming involved 50% of *ATL-N*. The rest of the area of this oceanic region had a slight warmth in its SST of less than 0.5 °C.



	NORTHERN HEMISPHERE				TROPICAL							SOUTHERN HEMISPHERE		
	PACIFIC			ATLANTIC	PACIFIC				ATLANTIC			PACIFIC	ATLANTIC	INDIAN
Statistic	*PAC-NE*	*NEP*	*PAC-NW*	*ATL-N*	*PAC-SC*	*NINO12*	*NINO3*	*NINO34*	*TNA*	*TSA*	*ATL-SC*	*PAC-S*	*ATL-S*	*IND-S*
Mean	1.28	1.04	0.77	0.50	−0.37	−0.38	−0.25	−0.10	0.21	0.17	0.12	0.01	0.21	−0.35
Standard Error	0.08	0.09	0.06	0.06	0.10	0.10	0.11	0.16	0.05	0.08	0.06	0.05	0.10	0.15
Median	1.26	1.01	0.73	0.55	−0.37	−0.52	−0.27	−0.13	0.26	−0.01	0.06	−0.03	0.09	−0.33
Standard Deviation	0.40	0.46	0.29	0.29	0.49	0.48	0.53	0.80	0.25	0.42	0.32	0.25	0.49	0.73
Variance	0.16	0.21	0.09	0.08	0.24	0.23	0.29	0.64	0.06	0.18	0.10	0.06	0.24	0.54
Kurtosis	0.01	−0.48	−0.03	−1.01	0.15	−0.87	−0.67	−1.66	−0.89	−0.47	−0.25	−0.26	1.36	0.64
Skewness	0.09	0.24	0.27	−0.10	0.34	0.39	−0.35	−0.12	0.03	0.58	0.13	−0.39	1.21	0.14
Range	1.64	1.76	1.27	0.94	2.01	1.68	1.80	2.23	0.93	1.60	1.36	0.93	1.90	3.26
Minimum	0.56	0.27	0.18	0.03	−1.30	−1.19	−1.28	−1.30	−0.22	−0.44	−0.54	−0.53	−0.52	−1.81
Maximum	2.21	2.02	1.45	0.97	0.71	0.49	0.52	0.93	0.72	1.16	0.82	0.41	1.38	1.45
Sum	31.89	25.89	19.24	12.60	−9.20	−9.46	−6.16	−2.53	5.16	4.16	2.95	0.33	5.22	−8.68
Count	25	25	25	25	25	25	25	25	25	25	25	25	25	25
Confidence Level (99.0%)	0.16	0.19	0.12	0.12	0.20	0.20	0.22	0.33	0.11	0.17	0.13	0.10	0.20	0.30

Figure 8. Mean Sea Surface Temperature Anomaly (SSTA, in °C) and resulting statistics for series June 2019/June 2021 at different oceanic regions and at different SST indexes (see Figure 2).

Now, besides such spatial SST dynamics, it is precisely in the northern oceanic regions of *PAC-NE*, *NEP*, *PAC-NW* and *ATL-N*, where the most significant warming trend was observed ($p < 0.01$, series January 1982/June 2021). Among these, the oceanic regions from the Northeast Pacific, *PAC-NE* and *NEP*, showed the strongest trend (Figure 9). An important contribution for such warming trend comes from two very distinctive SSTA positive pulses. The first one is a very extended SST warm pulse occurring from April 2013 until October 2016, lasting 43 months. The warming in this first pulse was less variable and significantly higher in *NEP* than in *PAC-NE* (1.02 vs. 0.84 °C, respectively; $p < 0.01$). As for the second Northeastern Pacific SST warming pulse, it started around April 2019 and, as for June 2021, still goes on (SSTA June 2021 = 1.35 and 0.84 °C, for *PAC-NE* and *NEP*, respectively), lasting until present, over 27 months. Differently than the first warm pulse, current pulse is significantly warmer at *PAC-NE* than at *NEP* (1.19 vs. 0.99 °C, respectively; $p < 0.01$). As for the Northwest Pacific, *PAC-NW*, this oceanic region has shown a very extended but variable warm SST pulse. With a mean of 0.69 °C, it was significantly less warm ($p < 0.05$) than Northeastern counterparts. The warm pulse in *PAC-NW* started in June 2017, way before current megadrought, and has lasted almost continuously until present (49 months). A brief pause in the anomalously positive condition in *PAC-NW* occurred in May 2019, little after *PAC-NE* and *NEP* started their second warming pulse (i.e., by April 2019). As for the Atlantic Ocean, the warming did not seem to respond to very extended intense SST warm pulses. For instance, most recent SST dynamic for *ATL-N* shows a rather mild pulse starting in January 2019 with a mean SST of only 0.48 °C. From Figure 9 it is also evident that SST warming dynamics in the long term has been generally significant for *TNA* ($p < 0.01$). But, such dynamics, differently than the other aforementioned oceanic regions, is rather discrete regarding most recent SST data: a warmth of only 0.36 °C was evident from January 2020 until March 2021.

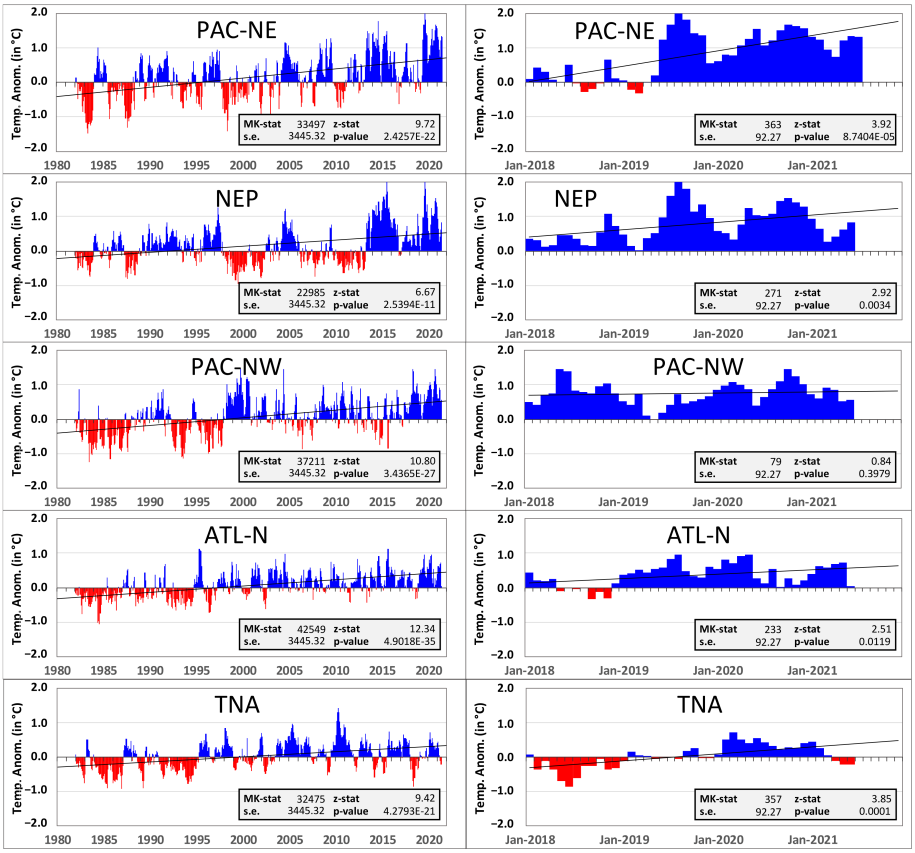


Figure 9. Sea Surface Temperature Anomalies (SSTA) for series January 1982/June 2021 at oceanic regions *PAC-NE*—Pacific Northeast, *PAC-NW*—Pacific Northwest and *ATL-N*—Atlantic North (see Figure 2). Anomalies are estimated from the monthly mean values of the series 1982–2011.

3.2.2. Marine Heatwave (MHW) Dynamics at the Northeast Pacific

Another important output from the temporal analysis of SST dynamics at the Northeast Pacific, besides its intensity, is regarding its duration. About this, Figure 10 shows that, for over two continuous years now (since June 2019/June 2021), SSTA at *PAC-NE* has been, not only well above the historic mean (climatological series January 1982/December 2011), but almost constantly above the 90th percentile. According to Hobday et al. [17], the combination of SSTA of such intensity and such persistence defines very well a Marine Heatwave (MHW) condition. In the case of *PAC-NE* current warming, the MHW condition has oscillated from the categories of moderate to about severe (Figure 10a). The MHW condition was also reached at *NEP* about the same time than in *PAC-NE* (by June 2019), but in a significantly ($p < 0.01$) lesser extent. As a matter of fact, while the MHW condition has persisted in *PAC-NE* until present (June 2021), at *NEP* it experienced a three-month break after February 2021 (Figure 10b).

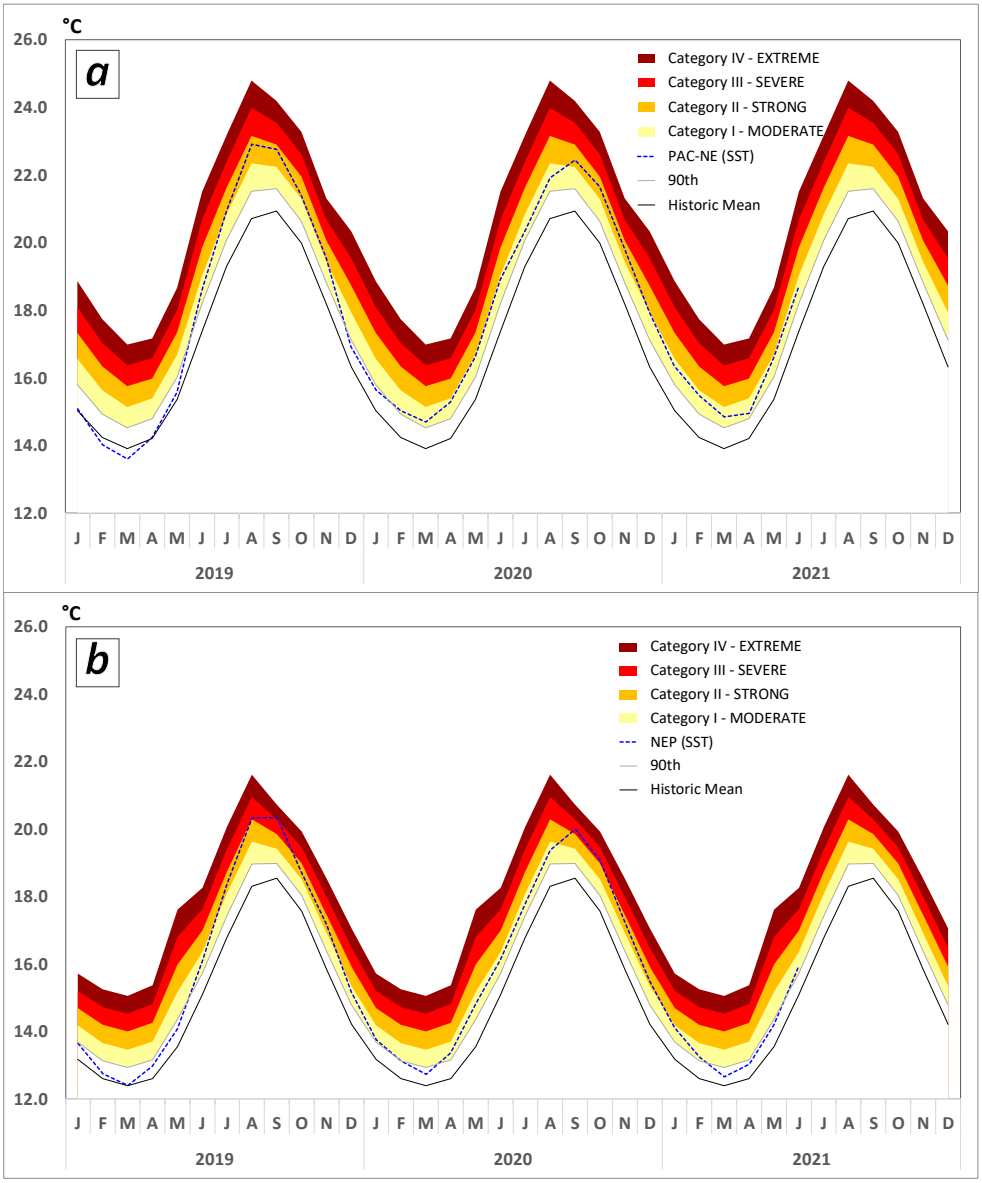


Figure 10. Most recent Marine heatwave (MHW) dynamics (from June 2019 to June 2021 and based on the SST series 1982–2011) at: (**a**) the *PAC-NE* oceanic region (from Thielen et al. [13]) and (**b**) the *NEP*—Northeast Pacific SST index region (from CPC/NCEP/NOAA [39] (see Figure 2). MHW categorization is taken from Hobday et al. [17].

As mentioned, two major warm SST pulses have occurred in the Northeast Pacific since January 1982 (see Figure 9). Such pulses generated two important and extended MHWs in both, *PAC-NE* and *NEP* (see Figure 11). No other oceanic regions, from those considered in the present study, showed MHW conditions of such intensity and/or duration. As for *NEP*, these two extreme warm pulses were identified in the present study as Blob 1 and Blob 2. Because 80% of *PAC-NE* is encompassed in *NEP*, for the purpose of the present study, the Blob 1 and Blob 2 are SST phenomena simultaneously occurring in *PAC-NE* and *NEP* (Figure 11a,b).

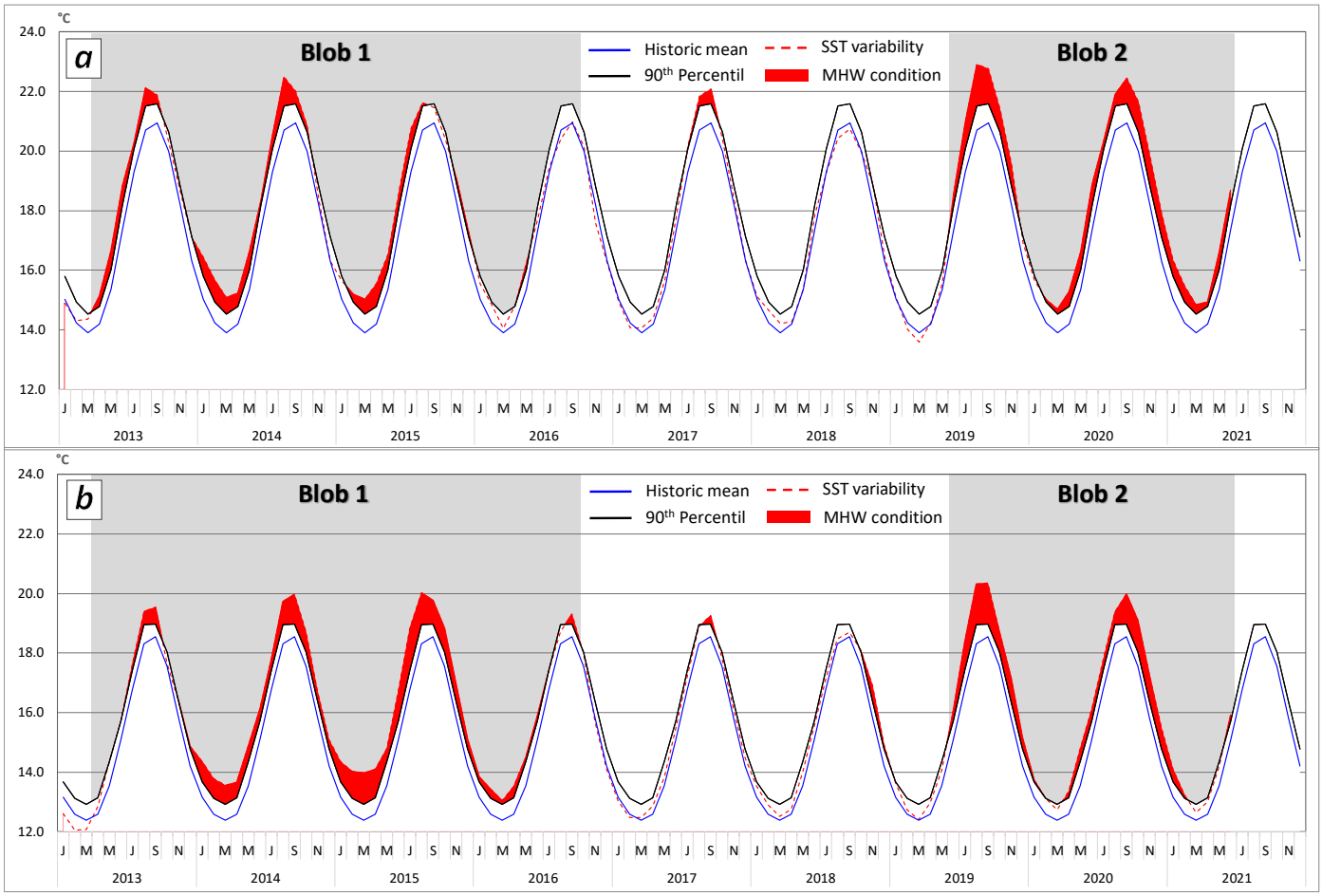


Figure 11. Marine heatwave (MHW) dynamics from January 2013 to June 2021 at: (**a**) the *PAC-NE* oceanic region (from Thielen et al. [13]) and (**b**) the region *NEP*—Northeast Pacific SST index (from CPC/NCEP/NOAA [39]) (see Figure 2). Solid blue line represents the historic mean SST for the climatological series January 1982—December 2011. As for the solid black line, it represents the 90th percentile, while the dashed red line represents the observed monthly SST variability. Red areas represent the moments when MHW condition has been reached (i.e., SSTA > 90th percentile). As for intensity, the thicker the resulting (red) area, the more intense the MHW. Grey areas are relative to the occurrence of Blob 1 and Blob 2.

Regarding Blob 1 dynamics, MHW condition during this extreme oceanic event was more persistent in *NEP* than in *PAC-NE*: Four breaks of two or three months at *PAC-NE*, versus only one two-month break occurred at *NEP*. As for Blob 2, although it is still an ongoing phenomenon, its MHW dynamics has been inversely that of Blob 1: more persistent in *PAC-NE* than in *NEP*, showing only a brief one-month break from the MHW condition.

3.3. Cross Correlating Monthly Precipitations with SST Dynamics

Besides expressing the highest SSTA, as well as showing the most persistent MHW condition, SST dynamics from *PAC-NE* correlates the best with precipitations anomalies

generating current megadrought at the UPRB. Results from cross correlating for the series June 2019/June 2021 show that, with a lead time of two months, SST at the *PAC-NE* significantly correlate ($p < 0.01$) with precipitations, explaining the ongoing megadrought condition: about 73.5% (for an $r = -0.8574$) in the case of the Pantanal, and 84.5% (for an $r = -0.9194$) for surrounding Highlands. Therefore, the warming trend observed in SST at *PAC-NE* implies a decrease in UPRB precipitation.

3.4. Megadrought's Forecast

From historical precipitation anomalies (series January 1981/June 2021) at the Pantanal and the surrounding Highlands (Figure 12a) and the application of time series forecasting techniques such as the Exponential Triple Smoothing (ETS), it is possible to make a projection of the megadrought. As shown in Figure 12b, negative precipitation anomalies (as SPDI) are expected at least until December 2023. Thus, current megadrought is expected to persist in the UPRB, severely affecting both, the Pantanal and the Highlands. In this time series forecasting, no significant difference was identified between observed vs. forecasted precipitation anomalies, in neither the Pantanal nor the Highlands (*t*-Test, $p = 0.3367$ and 0.6101, respectively).

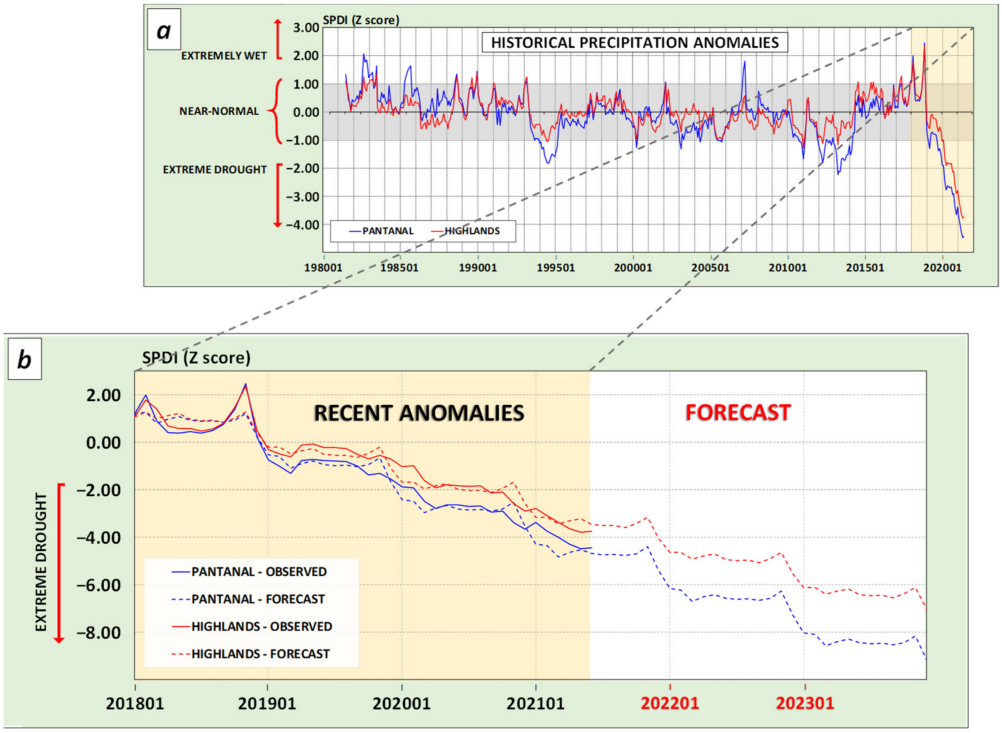


Figure 12. (**a**) Observed recent precipitation anomalies (as SPDI) for the series January 1981–June 2021 at the Pantanal and the surrounding Highlands. (**b**) Recent precipitation anomalies and time series forecasting for January 2021 to December 2023 by means of the Exponential Triple Smoothing (ETS).

4. Discussion

4.1. Megadrought's Evolution

The evolution of current megadrought has been differentiable in both, space and time. First evidence of a drought developing was observed right from the beginning of 2019 in the central section of the Pantanal. By mid-2019, an easterly spread of the drought occurred. And, in the term of nine months (by April 2020), over 60% of the area of the Pantanal, as well as 30% of the surrounding Highlands, succumbed to an extreme dry condition. Such extreme condition has persisted as a megadrought and, as for most recent update (June 2021), spreading over 80% of the Pantanal and about 60% of the Highlands. It is appropriate to classify the extreme event as a megadrought for this being very lengthy and

pervasive, as well as lasting much longer than any previous drought in the area [42] (see Figures 5–7 and 12).

In their analysis, which involves exclusively precipitations occurring at the Pantanal and only a segment of the megadrought (up to November 2020), Marengo et al. [20], referring to the initial dynamics of the drought, suggest a late onset of the rainy season (Oct–Mar) of the hydrological year 2019–2020 with a rainfall deficit of 40%. In the present study, such deficit was prominently lower (23%). A deficit which was not sensibly different from that generated during the next rainy season of 2020/2021 (17%). Now, the origin of the differences between the results from both studies may lay in the extension of the series involved.

At the Pantanal, dry spells have been significantly more frequent than wet ones. Three main dry spells have occurred in the Pantanal in the last 40 years. The first one is a moderate drought lasting 15 uninterrupted months (September 1993/November 1994), while the second dry spell lasted 14 continuous months (January 2013/February 2014) and generated a severe drought in the Pantanal. Although historically dry spells have not affected the surrounding Highlands [13], is it during the third and last dry spell—the current megadrought—that negative precipitation anomalies not only affected the Pantanal, but the surrounding Highlands as well. Nevertheless, the megadrought temporal dynamics along the UPRB was differentiable—the drought condition was reached four months' sooner in the lowlands of the Pantanal than in the higher lands of the surrounding Cerrado (September 2019 and January 2020, respectively).

4.2. SSTA Dynamics and Resulting MHWs

Since mid-2019, and about simultaneously to the dramatic spread of the megadrought in the UPRB (with a lead of two months), a very important warming of Northern Hemisphere oceanic waters has been in process. More specifically, in the oceanic regions of *PAC-NE*, *PAC-NW* and *ATL-N*, previously identified by Thielen et al. [13]. Such warming has been most significantly intense and extended in waters of the Northeast Pacific, involving both, *PAC-NE*, and *NEP*. No other oceanic region, from those considered in the present study, showed SSTA dynamics, for warming (or even for cooling) as intense and/or as enduring as that observed in the Northeast Pacific since mid-2019.

Such dynamics of SSTA is precisely what describes a MHW—A discrete period of prolonged anomalously warm water at a particular location, exceeding a fixed [43], seasonally varying [44], or cumulative [45] threshold. The MHW condition is specifically reached when SSTA not only surpasses the historical mean but above the 90th percentile [17]. Short lasting MHWs (over few days) may disturb the marine environment, it is the long-lasting events that have the most significant impact [46]. With only a short one-month break at the end of 2019, *PAC-NE* has constantly reached the MHW condition since June 2019. The MHW condition has been significantly higher and more persistent in *PAC-NE* than in *NEP*. Such persistence of a MHW at the Northeast Pacific was also referred by the reports from Global Ocean Monitoring and Observing Program (GOMO), ratifying the MHW condition for the Northeast Pacific in its report of 12 July 2021 [39].

Results also show that observed SSTA dynamics and resulting MHWs at the Northeast Pacific is part of a generalized warming trend of the Northern Hemisphere oceanic waters. While for the Atlantic Ocean such trend has been rather gradual since 1982, for the Pacific this has been more accentuated from the beginning of the 21st century (as for *PAC-NW*), and most extreme this last decade for eastern side of the North Pacific (as for *PAC-NE* and *NEP*). In the case of Northeast Pacific, an important contribution for such warming trend came from two very distinctive MHWs. The first one, is a very extended SST warm pulse occurring from April 2013 until October 2016, lasting 43 months. Originally known by the moniker of "The Blob" in the general press [47]—as Blob 1, in the present research. As for the second northeastern Pacific MHW, Blob 2 (after Amaya et al. [48]), it started around April 2019 and still goes on lasting, as for June 2021, over 27 months. Up to this point, the warming dynamics during Blob 1 and Blob 2 has been distinctive, not only between these

two important MHWs, but between the oceanic regions of *PAC-NE* and *NEP*. For instance, during Blob 1, SSTA was less variable and significantly higher in *NEP* than in *PAC-NE*, while the opposite has been true during the ongoing Blob 2. Blob 1 is the largest and longest MHW ever recorded between 1981 to 2017, not only for *NEP*, but in general [49–51]. Now, because Blob 2 is an ongoing process and, as for June 2021, there is no sign of a soon end, much from this important MHW event is still be expected.

The participation of the different climate modes modulating the frequency, intensity and duration of the different MHWs is still under great debate [44,52]. The Pacific Decadal Oscillation (PDO), the North Pacific Gyre Oscillation (NPGO), El Niño-Southern-Oscillation (ENSO), among others, influence ocean temperatures and thus the development of MHWs, directly or remotely via atmospheric or oceanic teleconnections, which reverberate the effects globally [53]. As for potential drivers of Blob 1, there has been identified a link to the dynamics of the two dominant modes of winter sea surface temperature variability in the North Pacific, the Pacific Decadal Oscillation (PDO), and the North Pacific Gyre Oscillation (NPGO) [52,54]. Specifically, between winter warm NPGO anomalies and the following winter PDO arising from extratropical/tropical teleconnections. But, unlike Blob 1, Blob 2 peaked in the summer, a season when little is known about the physical drivers of such events [48]. According to these authors, Blob 2 primarily results from a prolonged weakening of the North Pacific High-Pressure System, which reduces surface winds and decreases evaporative cooling and wind-driven upper ocean mixing. Warmer ocean conditions then reduce low-cloud fraction, reinforcing the MHW through a positive low-cloud feedback. Amaya et al. [48] also found that remote SST forcing from the central equatorial and, surprisingly, the subtropical North Pacific Ocean contribute to the weakened North Pacific High. This study also highlighted the possibility that, due to resulting Northeast Pacific mixed layer depths extremely shallow, Blob 2 would not last much longer than winter and spring 2020 seasons. Results from present study show that, even though the MHW condition at *PAC-NE* and *NEP* did weaken and even disappeared for a couple of months during that time, as for *PAC-NE*, the MHW condition was not only reestablished and has persisted until present, with no evidence of weakening. This result reinforces the importance not only to identify the drivers capable of initiating MHWs at different seasons [48], but also about the necessity of evaluate potential alternating dynamics, intra e inter annually, among the different drivers capable of determining the life-span and intensity of important foreseeable MHWs occurring at the Northeast Pacific.

4.3. Cross Correlations between Monthly Precipitations and SST Dynamics

Even though the exact mechanisms for how SST may influence precipitation at a local level was not considered in this study, the application of correlation analysis on different hydrological indices and SST data permits the identification of regions where the interactions between hydrological droughts and teleconnection are strong [40]. As a consequence of aforementioned Blob 2 (i.e., an extended SST warm pulse occurring at the Northeast Pacific), a very persistent and intense MHW condition was generated at the oceanic region *PAC-NE* and the associated *NEP* right from June 2019, which is the same moment identified in the present study as the beginning of current megadrought. The results from lagged correlation between the monthly mean precipitations at the Pantanal and the surrounding Highlands with monthly SST at the different oceanic regions analysis show that, for the series June 2019/June 2021 and with a two-month offset (lead time), it is *PAC-NE*'s MHW condition that best correlates and explains, right from the beginning of the megadrought, the precipitation anomalies at the UPRB: 73.5% in the case of the Pantanal, and 84.5% for surrounding Highlands.

As for the rest of the oceanic regions considered in the present study: from the tropics (i.e., *PAC-SAC*—Pacific South American Coast, and the ENSO regions: *NIÑO 1+2*, *NIÑO 3* and *NIÑO 3.4*), as well as from the Southern Hemisphere (i.e., *ATL-SC*—Atlantic South Central, *ATL-S*—Atlantic South, *PAC-S*—Pacific South, and *IND-S*—Indian South), and even referential SST indexes such as *TNA*—Tropical North Atlantic and *TSA*—Tropical

South Atlantic; all these failed explain the megadrought dynamics as significantly as did the Northeast Pacific region of *PAC-NE*. In these terms, a warming trend in SST at *PAC-NE* and the concomitant presence of a MHW implies a decrease in UPRB precipitations, with the possibility of generating a megadrought condition. Nevertheless, because the existence of a significant correlation between the SST of the other two Northern Hemisphere oceanic regions—*PAC-NW* in the West Pacific and *ATL-N* in North Atlantic—and the historical dynamics in the precipitations of the Pantanal [13], there is also the possibility of future megadroughts resulting from current warming trend observed in these two specific oceanic areas.

Evaluating the potential causes of the precipitation deficit from the austral summer (December 2019/February 2020) at the Pantanal, Marengo et al. [20] propose that it was caused by a reduction in the transport of warm and humid (austral) summer air from Amazonia into the Pantanal. These authors suggest that such event occurred in association with an anomalous warming of the Atlantic Ocean captured by the AMO and *TNA* indices, inducing an anomalously northward position of the Atlantic ITCZ, producing less rainfall in southern Amazonia and the Pantanal. But, Marengo et al. [20] also found that other drought episodes in the Pantanal not necessarily follow this pattern. Regarding this possibility, the outcomes from the present study, which include analysis from the second and most recent austral summer from current megadrought (December 2020/February 2021), show that, due to the generalized but significant warming trend observed in the North Atlantic, as for oceanic regions such as *ATL-N* and *TNA*, SSTA for last austral summer (December 2020/February 2021) did was higher than for the preceding (December 2019/February 2020). But, regardless of such warmth difference (+0.18 °C and +0.38 °C, in the case of *TNA*), no significant concomitant response in precipitation anomaly was detected among the two austral summers, as would be expected.

Regarding major SST based indices such as *TNA*, AMO, PDO, and ONI, Marengo et al. [20] identified a very low correlation between rainfall in the Pantanal, as well as Paraguay River level at Ladário and SST dynamics. The results from present research, not only agrees with such findings, but provides information about the specific areas, encompassed in the very extended ocean sections where these and other macroclimate indices express their SST dynamics at different time scales, from interannual to interdecadal, and expressing the highest correlation with precipitation dynamics at the UPRB, not only at different time scales, but also at different space scales. About this last issue, Batista Silva et al. [55] established that, with a lead of 3 months and explaining 66% of the monthly variance, PDO negative phases concomitantly occurred with drier periods in the Pantanal. Now, according to CPC/NCEP/NOAA [39], as for June 2021, the PDO phase is negative and has persisted so since January 2020. Thus, current negative phase of PDO fails, by itself, to fully explain current megadrought dynamics, right from its beginning in June 2019. Now, results from present study show that, when using in this kind of correlation analysis a more specific and targeted oceanic region, as resulted to be *PAC-NE* explaining precipitation variability at the UPRB, the lead time for response shortens (2 months), as well as sensibly improves the capacity to explain (74–85%) any resulting drought, both in time and in space, and all along the evolution, not only of current megadrought, but of other recent important drought events.

One of such events occurred during 2013 and part of 2014. South America was experiencing an important drought at about the same time of the so-called "second dry spell" of the Pantanal, described earlier in this study (see Section 4.1). Now, according to Rodrigues et al. [56,57], such dry condition was generated by an unprecedented MHW developed in a rather small and specific area of the western South Atlantic that lasted for almost all of the summer (<4 months), which apparently suppressed the South Atlantic convergence zone and its associated rainfall. Regarding this specific MHW, from the three South Atlantic related oceanic regions considered in the present study (i.e., *ATL-SC*, *ATL-S* and *TSA*), only *ATL-S* showed a moderate MHW condition, lasting only 3 months (February/April 2014). As for the specific South Atlantic oceanic region indicated by

Rodrigues et al. [56], resulting SSTA and MHW dynamics do not explain satisfactorily the drought in the Pantanal since, by the time the warming of SST occurs and the short-lived MHW reaches its maximum (by February 2014), the severe dry condition was already affecting the Pantanal for over a year (since February 2013). Results from the present study regarding the presence of warm SST at the Northeast Pacific and the presence of Blob 2 and the concomitant generation and dynamics of a MHW at *PAC-NE*, provide the solid arguments as to explain this particular 2013/2014 dry spell from the concurrent presence of Blob 1 at the Northeast Pacific and the generation of a persistent and intense MHW at *NEP*. An explanation that points out to the most probable origin of such specific dry spell in the Pantanal, as might explain also, the origin of a more extended climatic phenomenon, such as the generalized drought concomitantly affecting vast areas of South America. Results from present study leave solid open grounds as for the (re)evaluation the origin and dynamics, not only extreme droughts that have affected extended regions along history, but also more recent and even ongoing extreme dry events such as the drought that is currently spreading and intensifying across South America [58].

4.4. Megadrought's Forecast

The application of time series forecasting techniques to historical precipitation allowed to make a projection of the ongoing megadrought affecting the UPRB. Results from present study show that the dry condition (as negative precipitation anomalies) is expected at both the Pantanal and the surrounding Highlands at least until December 2023. Even if precipitation amounts normalize from this point on, it would take over 30 continuous months as for any drought condition to disappear in the Pantanal area. Now, the sooner the current extreme drought condition can become about normal is if, at both the Pantanal and the surrounding Highlands, each month of next rainy season (i.e., October 2021/March 2022) reaches a relative positive anomaly of 43% or above from historical mean (series 1981–2020). A positive anomaly of such magnitude has never been reached in the Upper Paraguay river basin at least for the last 40 years. For instance, the wettest rainy season (i.e., October 2016/March 2017) presented an anomaly of 21% above historical mean, that is less than half the amount of rain currently demanded.

Even though fire is considered a natural disturbance in the Neotropical savannas, in the case of the Pantanal, due to its wetter condition, fires here have been historically less frequent and spatially restricted [26,59]. However, given the ongoing megadrought, reductions in precipitation are still expected to cause significant disturbances in its ecological functioning, affecting hydrological, floodplain inundation dynamics, as well as fire regime. The intensification of fire risk, extending now to areas historically flooded or perhumid, is expected. Concomitantly, and as predicted by Thielen et al. [26], it is likely a negative impact on non-fire-resistant vegetation cover, as well as ecosystem functioning and biodiversity, perhaps even worse than those from 2020.

Now, according to the latest report from the Global Water Monitor and Forecast Watch List (15 July 2021, [58]) which provides a 12-month prediction through March 2022 indicate that exceptional deficits are forecasted not only along the Paraguay River through its namesake, but also along the Paraná River through Brazil, Paraguay, and Argentina. As mentioned in the previous section, the exceptional drought is becoming a generalized condition in many parts of South America, a condition that is expected to keep spreading. From preliminary estimations, we found that 22% of South America is currently under a drought as severe as the one currently affecting the Pantanal. With 82% of its area, Pantanal is the biome most affected by the megadrought, followed by the Mata Atlântica (55%), the Cerrado (37%), Caatinga (16%) and Amazônia (9%). As for Brazil, 35% of its territory is currently under different degrees of droughts, from which 23% is extreme. According to Parris [58], widespread water deficits ranging from severe to exceptional are expected in the states of Mato Grosso, Mato Grosso do Sul, São Paulo, and Paraná. Deficits reaching exceptional intensity are forecast for parts of western Amazonas and Acre, Pará and Amapá, and Maranhão. Regarding SSTA forecasts, the Climate Forecast System of

the National Centers for Environmental Predictions [39] recognized that initial projections underestimated the strength of current Northeast Pacific MHW and suggested that the MHW condition in this oceanic region should continue for the next 6 months.

As mentioned, the projection of the present study is founded on consideration to historical variability, status and trends of precipitation and the SSTs from several oceanic regions, specific to the series June 2019–June 2021 and based in the climatological January 1981–December 2011. Any case, further drought projections should be reevaluated in terms of the newly identified causal connections between the Pantanal dry pulses and the increasing Northern Hemisphere SST and foreseeable increase in occurrence MHWs [13,26]. This adjustment would allow to determine whether predicted conditions are consistent and supported by current data and models or whether these conditions indicate larger scales and more complex climate dynamics. The correlations between precipitations at the UPRB with more than one oceanic region stresses the importance of future studies evaluating combined influence [13,20].

Regarding MHWs, even though knowledge about their functioning, drivers, impacts and future evolution, is still in its infancy [44,52,60], consensus is emerging that anthropogenic climate change has significantly increased the likelihood of recent MHWs, especially for the more extreme category events [15,16,18,51]. Frölicher et al. [43] found that MHW duration doubled from 1982 to 2016 and attributed 87% of MHWs to human-induced warming. Significant increases in MHW intensity and count of annual MHW days are projected to accelerate, with many parts of the ocean reaching a near-permanent MHW state by the late 21st century [18].

Improved skill to predict oceanographic conditions in the North Pacific is highly desirable [61]. Blob 1's warmth penetrated hundreds of meters below the surface, but Blob 2's has not reached such depth yet [48]. To answer how long will Blob 2 last is a matter of knowing how deep its warmth will penetrate below the surface. This kind of information would improve drought forecasting capacity for the Pantanal, and even for extended regions of South America, since both Blob 1 and Blob 2 have proven capacity of generating extreme MHW conditions in *PAC-NE* as well as in *NEP*, an oceanic phenomenon that is strongly correlated with the occurrence and dynamics of extreme droughts in the Pantanal and surrounding areas. Now, in the last quarter of this decade, global ocean heat gain has increased in the upper 700 m of the ocean and heat has been sequestered in deeper ocean layers at depths down to more than 2000 m [62]. Ocean Heat Content refers to the heat absorbed by the ocean. More than 90% of the excess heat is stored within the world's oceans, where it accumulates and causes increases in ocean temperature [63,64]. Knowing how much heat energy is stored in the ocean—and where it is stored and released—is essential for understanding the state, variability, and changes of Earth's climate system [62,65]. The gradual buildup of subsurface heat content throughout 2020 in the region suggests the potential for persistent ecological impacts [66]. As warmer temperatures gradually mix downward, they can persist long after the surface MHW disappears, suggesting that the ocean can provide memory for long-lived MHWs [66]. The stronger ocean warming within upper layers versus deep water has caused an increase of ocean stratification in the past half century [67]. With increased stratification, heat from climate warming less effectively penetrates into the deep ocean, which contributes to further surface warming [68].

As for 2019, the world's oceans (especially the upper 2000 m) were the warmest in recorded human history [69]. Due to resulting teleconnections, this is one of the key reasons why the Earth experienced such catastrophic fires in the Amazon, California, and Australia in 2019 [65]. An update for this list would have to include the unprecedented fires in the Pantanal, for 2020, and upcoming years until the precipitation siege from MHW at *PAC-NE* ceases. It is important to note that ocean warming will continue even if the global mean surface air temperature can be stabilized at or below 2 °C (the key policy target of the Paris Agreement) in the 21st century [64,65,70]. The ocean, and some other components in the Earth system, are slow to respond and equilibrate, and will continue to change even after radiative forcing stabilizes [64]. However, the rates and magnitudes of ocean

warming, and the associated risks will be smaller with lower levels of anthropogenic GHG emissions [64,65,70].

5. Conclusions

The present study generates reliable information about three key issues: 1—Megadrought's evolution and dynamics, 2—Megadrought's origin and determinants, and 3—A forecast based on identified determinants and current trends.

1. The evolution of the megadrought currently affecting the Pantanal has been differentiable in both, space and time. First evidence of a drought developing was observed in the central section of the Pantanal, right from the beginning of 2019. By mid-2019, an easterly spread of the drought occurred, and as for June 2021, over 80% of the Pantanal area and about 60% of the Highlands is affected by the megadrought. As for temporal dynamics, the drought condition was reached four months' sooner in the lowlands of the Pantanal than in the surrounding higher lands.
2. The study ratifies that Climate Change is one of the most important threats to the Pantanal. The evolution and dynamics of current megadrought is correlated to a significant warming trend of the Northeast Pacific sea surface waters (SST) which resulted, since June 2019, in one of the most intense and persistent marine heatwave (MHW) from recent times, identified by other authors as Blob 2. The present study also provides evidence that Blob 1, a preceding MHW also from the Northeast Pacific strongly correlates to the second most important drought (2013–2016) occurred in the Pantanal area in the last 40 years. Encompassed in the Northeast Pacific, the SST warming of *PAC-NE* region explains, right from the beginning of the megadrought, 73.5% of the precipitation anomalies in the case of the Pantanal, and 84.5% for surrounding Highlands. As for South American neighboring oceanic regions (e.g., TNA, TSA and the ENSO regions), their SST dynamics was rather discrete, and did not explain Pantanal's megadrought in the terms as did the presence of a MHW in the Northeast Pacific. Now, the SST warming trend at the Northeast Pacific is part of a generalized warming trend of the Northern Hemisphere oceanic waters. There is a historical correlation between the presence of warm SST at *PAC-NW* in the Northwest Pacific and *ATL-N* in the North Atlantic and the occurrence of dry pulses in the Pantanal area.
3. Pervasive MHWs from warming oceanic waters of the Northern Hemisphere—The "new climatic reality" that the Pantanal and other vast regions of South America have to overcome. Results from this study as well as from others provide arguments as to consider the problematic of warmer SST as a new climatic reality. Anthropogenic climate change has significantly increased the likelihood of recent MHWs, especially for the more extreme category events. Blob 2 is an ongoing process with no signs to end any soon. Blob 1's warmth penetrated hundreds of meters below the surface, but Blob 2's has not reach such depth yet. To answer how long will Blob 2 last, ergo the megadrought, is a matter of knowing how deep will its warmth penetrate below the surface. In addition, and because the existence of a significant correlation between the SST dynamics of the other two Northern Hemisphere oceanic regions (i.e., *PAC-NW* and *ATL-N*) and the historical dynamics in the precipitations of the Pantanal, there is also the possibility of future megadroughts resulting from current warming trend and potential MHWs generating in these two oceanic areas. Regarding a forecast for the megadrought, results from present study show that it is expected to continue at both the Pantanal and the surrounding Highlands at least until December 2023. Even if precipitation amounts normalize from this point on, it would take over 30 continuous months as for any drought condition to disappear in the Pantanal area. The sooner the current extreme drought condition can become about normal is if, at both the Pantanal and the surrounding Highlands, each month of next rainy season (i.e., October 2021/March 2022) reaches a relative positive anomaly of 43% or above from historical mean (series 1981–2020). But a positive anomaly of such

magnitude has never been reached in the Upper Paraguay river basin at least in the last 40 years. Due to the continuity of the megadrought, the intensification of fires with unprecedented duration and intensity, extending now to areas historically flooded or perhumid are expected. Concomitantly, we predict a most definite negative impact on non-fire-resistant vegetation cover, as well as ecosystem functioning and biodiversity, perhaps even worse than those from 2020.

Now, the exceptional drought is becoming a generalized condition in many parts of South America. From preliminary own estimations, about 22% of South America is currently under a drought as severe as the megadrought affecting the Pantanal. With 82% of its area, Pantanal is the biome most affected by the megadrought, followed by the Mata Atlântica (55%), the Cerrado (37%), Caatinga (16%) and Amazônia (9%). Here, the exceptional drought condition is expected to keep spreading.

The present study provides valuable and reliable skills as to deal with key issues about such abrupt and extreme drought, providing to decision-makers, stakeholders and society most useful and opportune information regarding its origin, evolution and a forecast based on identified determinants and current trends. Any case, further drought projections should be reevaluated in terms of the newly identified causal connections between the dry pulse's dynamics and the increasing Northern Hemisphere SST and foreseeable increase in occurrence MHWs.

Author Contributions: Conceptualization, D.T., P.R.-P. and R.L.; methodology, D.T. and P.R.-P.; software, D.T.; formal analysis, D.T., P.R.-P., M.L.P., M.M., J.I.Q., W.R., A.S.-W., K.T. and A.N.; data curation, D.T., P.R.-P. and M.L.P.; writing—original draft preparation, D.T.; writing—review and editing, D.T., P.R.-P. and R.L.; visualization, D.T. and P.R.-P.; supervision, D.T. and P.R.-P.; project administration, D.T.; funding acquisition, R.L. All authors have read and agreed to the published version of the manuscript.

Funding: This work was funded by Pantanal Research Network (FINEP grant 01.20.0201.00) from MCTI. R.L. was funded by FAPERJ (Grant E26/202.714/2019) and by CNPq [grant 305159/2018–6].

Institutional Review Board Statement: Not applicable.

Informed Consent Statement: Not applicable.

Data Availability Statement: Precipitation data was freely provided by the Climate Hazards group Infrared Precipitation with Stations at https://iridl.ldeo.columbia.edu/SOURCES/.UCSB/.CHIRPS/.v2p0/.monthly/.global/ (accessed on 10 October 2021). As for the monthly SST data, this was freely provided by the NOAA at http://iridl.ldeo.columbia.edu/maproom/Global/Ocean_Temp/Monthly_Temp.html (accessed on 10 October 2021).

Acknowledgments: Grants from the Organization of American States by the Programa de Alianças para a Educação e a Capacitação (Bolsas Brasil—PAEC OEA-GCUB) were assigned to P.R.P. and A.S.-W., allowing their continuous and important participation in the present research. The access to GIS software was provided by Service Unit of Geographical System Information (UniSIG), Ecology Center of the Venezuelan Institute for Scientific Research (IVIC), Caracas, Venezuela. Finally, the authors wish to thank the anonymous reviewers for their recommendations which resulted in a significant improvement of the present work.

Conflicts of Interest: The authors declare no conflict of interest. The funders had no role in the design of the study; in the collection, analyses, or interpretation of data; in the writing of the manuscript, or in the decision to publish the results.

References

1. Alho, C.J.R.; Lacher, T.E., Jr.; Gonçalves, H.C. Environmental Degradation in the Pantanal Ecosystem. *BioScience* **1988**, *38*, 164–171. [CrossRef]
2. Mittermeier, R.A.; de Gusmao Camara, I.; Tereza, M.; Padua, J.; Blanck, J. Conservation in the Pantanal of Brazil. *Oryx* **1990**, *24*, 103–112. [CrossRef]
3. Por, F.D. *The Pantanal of Mato Grosso (Brazil)—World's Largest Wetlands*; Kluwer Academic: Dordrecht, The Netherlands, 1995; pp. 1–3.

4. Alho, C.J.R.; Silva, J.S.V. Effects of severe floods and droughts on wildlife of the Pantanal wetland (Brazil)—A review. *Animals* **2012**, *2*, 591–610. [CrossRef] [PubMed]
5. Girard, P. The Pantaneiros, perceptions and conflicts about the environment in the Pantanal in Tropical wetland management. In *Tropical Wetland Management: The South-American Pantanal and International Experience*; Ioris, A.A.R., Ed.; Ashgate Publishing: London, UK, 2012.
6. Junk, W.J. Flood pulsing and the linkages between terrestrial, aquatic, and wetland systems. *Verh. Internat. Verein. Theor. Angew. Limnol Verhandlungen* **2005**, *29*, 11–38. [CrossRef]
7. Alho, C.J.R.; Sabino, J. Seasonal Pantanal flood pulse: Implications for biodiversity conservation—A Review. *Oecol. Aust.* **2012**, *16*, 958–978. [CrossRef]
8. Bergier, I.; Assine, M.L.; McGlue, M.M.; Alhod, C.J.R.; Silva, A.; Guerreiro, R.L.; Carvalho, J.C. Amazon rainforest modulation of water security in the Pantanal wetland. *Sci. Total Environ.* **2017**, *619–620*, 1116–1125. [CrossRef]
9. Erwin, K.L. Wetlands and global climate change: The role of wetland restoration in a changing world. *Wetl. Ecol. Manag.* **2009**, *17*, 71–84. [CrossRef]
10. Junk, W.J. Current state of knowledge regarding South America wetlands and their future under global climate change. *Aquat. Sci.* **2013**, *75*, 113–131. [CrossRef]
11. Bergier, I. Effects of highland land-use over lowlands of the Brazilian Pantanal. *Sci. Total Environ.* **2013**, *463–464*, 1060–1066. [CrossRef]
12. Ioris, A.A.R.; Irigaray, C.T.; Girard, P. Institutional responses to climate change: Opportunities and barriers for adaptation in the Pantanal and the Upper Paraguay River Basin. *Clim. Chang.* **2014**, *127*, 139–151. [CrossRef]
13. Thielen, D.; Schuchmann, K.-L.; Ramoni-Perazzi, P.; Marquez, M.; Rojas, W.; Quintero, J.I.; Marques, M.I. Quo vadis Pantanal? Expected precipitation extremes and drought dynamics from changing sea surface temperature. *PLoS ONE* **2020**, *15*, e0227437. [CrossRef]
14. Alexander, M.A.; Scott, J.D.; Friedland, K.D.; Mills, K.E.; Nye, J.A.; Pershing, A.J.; Thomas, A.C. Projected sea surface temperatures over the 21st century: Changes in the mean, variability and extremes for large marine ecosystem regions of Northern Oceans. *Elem.-Sci. Anthrop.* **2018**, *6*, 9. [CrossRef]
15. Schlegel, R.W.; Oliver, E.C.J.; Hobday, A.J.; Smit, A.J. Detecting Marine Heatwaves with Sub-Optimal Data. *Front. Mar. Sci.* **2019**, *6*, 737. [CrossRef]
16. Oliver, E.C.J.; Donat, M.G.; Burrows, M.T.; Moore, P.J.; Smale, D.A.; Alexander, L.V.; Benthuysen, J.A.; Feng, M.; Gupta, A.S.; Hobday, A.J.; et al. Longer and more frequent marine heatwaves over the past century. *Nat. Commun.* **2018**, *9*, 1324. [CrossRef]
17. Hobday, A.J.; Oliver, E.C.J.; Gupta, A.S.; Benthuysen, J.A.; Burrows, M.T.; Donat, M.G.; Holbrook, N.J.; Moore, P.J.; Thomsen, M.S.; Wernberg, T.; et al. Categorizing and naming marine heatwaves. *Oceanography* **2018**, *31*, 162–173. [CrossRef]
18. Oliver, E.C.J.; Burrows, M.T.; Donat, M.G.; Gupta, A.S.; Alexander, L.V.; Perkins-Kirkpatrick, S.E.; Benthuysen, J.A.; Hobday, A.J.; Holbrook, N.J.; Moore, P.J.; et al. Projected Marine Heatwaves in the 21st Century and the Potential for Ecological Impact. *Front. Mar. Sci.* **2019**, *6*, 734. [CrossRef]
19. Marinha do Brasil. Centro de Hidrografía e Navegação do Oeste—Ladário 2016–2021. Available online: https://www.marinha.mil.br/chn-6/sites/www.marinha.mil.br.chn-6/files/3-LADÁRIO%2009.pdf (accessed on 18 July 2021).
20. Marengo, J.A.; Cunha, A.P.; Cuartas, L.A.; Leal, K.R.D.; Broedel, E.; Seluchi, M.E.; Michelin, C.M.; Baião, C.F.D.P.; Ângulo, E.C.; Almeida, E.K.; et al. Extreme Drought in the Brazilian Pantanal in 2019–2020: Characterization, Causes, and Impacts. *Front. Water* **2021**, *3*, 639204. [CrossRef]
21. Libonati, R.; Pereira, J.M.C.; Camara, C.C.D.; Peres, L.F.; Oom, D.; Rodrigues, J.A.; Santos, F.L.M.; Trigo, R.M.; Gouveia, C.M.P.; Machado-Silva, F.; et al. Twenty-first century droughts have not increasingly exacerbated fire season severity in the Brazilian Amazon. *Sci. Rep.* **2021**, *11*, 4400. [CrossRef]
22. Hassan, W.U.; Nayak, M.A. Global teleconnections in droughts caused by oceanic and atmospheric circulation patterns. *Environ. Res. Lett.* **2021**, *16*, 014007. [CrossRef]
23. Libonati, R.; DaCamara, C.C.; Peres, L.F.; Carvalho, L.A.S.D.; Garcia, L.C. Rescue Brazil's burning Pantanal wetlands. *Nature* **2020**, *588*, 217–219. [CrossRef]
24. Garcia, L.C.; Szabo, J.K.; Roque, F.D.O.; Pereira, A.D.M.M.; Cunha, C.N.D.; Damasceno-Júnior, G.A.; Morato, R.G.; Tomas, W.M.; Libonati, R.; Ribeiro, D.B. Record-breaking wildfires in the world's largest continuous tropical wetland: Integrative fire management is urgently needed for both biodiversity and humans. *J. Environ. Manag.* **2021**, *293*, 112870. [CrossRef]
25. Filho, W.L.; Azeiteiro, U.M.; Salvia, A.L.; Fritzen, B.; Libonati, R. Fire in Paradise: Why the Pantanal is burning. *Environ. Sci. Policy* **2021**, *123*, 31–34. [CrossRef]
26. Thielen, D.; Ramoni-Perazzi, P.; Marquez, M.; Quintero, J.I.; Rojas, W.; Puche, M.L.; Soto-Werschitz, I.A.; Thielen, K.; Nunes, A.; Libonati, R. Marine heatwaves in the dynamics of the Pantanal's historical drought and unprecedented fires. In Proceedings of the EGU General Assembly 2021, Wien, Austria, 26–30 April 2021; p. EGU21-9268. [CrossRef]
27. Berlinck, C.N.; Lima, L.H.A.; Pereira, A.M.M.; Carvalho, E.A.R., Jr.; Paula, R.C.; Thomas, W.M.; Morato, R.G. The Pantanal is on fire and only a sustainable agenda can save the largest wetland in the world. *Braz. J. Biol.* **2021**, *82*, 2022. [CrossRef]
28. Assine, M.L.; Merino, E.R.; Pupim, F.N.; Warren, L.V.; Guerreiro, R.L.; McGlue, M.M. Geology and Geomorphology of the Pantanal Basin. In *Dynamics of the Pantanal Wetland in South America*; Bergier, I., Assine, M.L., Eds.; Springer International Publishing: Cham, Switzerland, 2015; pp. 23–50. [CrossRef]

29. Silva, J.D.S.V.; Abdon, M.D.M. Delimitacão do Pantanal brasileiro e suas sub-regiões. *Pesqui. Agropecu. Bras.* **1998**, *33*, 1703–1711.
30. Funk, C.; Peterson, P.; Landsfeld, M.; Pedreros, D.; Verdin, J.; Shukla, S.; Husak, G.; Rowland, J.; Harrison, L.; Hoell, A.; et al. The climate hazards infrared precipitation with stations—A new environmental record for monitoring extremes. *Sci. Data* **2015**, *2*, 150066. [CrossRef] [PubMed]
31. Beck, H.E.; Vergopolan, N.; Pan, M.; Levizzani, V.; Dijk, A.I.J.M.V.; Weedon, G.; Brocca, L.; Pappenberger, F.; Huffman, G.J.; Wood, E.F. Global-scale evaluation of 23 precipitation datasets using gauge observations and hydrological modeling. *Hydrol. Earth Syst. Sci.* **2017**, *21*, 6201–6217. [CrossRef]
32. Bulgin, C.E.; Merchant, C.J.; Ferreira, D. Tendencies, variability and persistence of sea surface temperature anomalies. *Sci. Rep.* **2020**, *10*, 7986. [CrossRef] [PubMed]
33. Pita López, M.F. Un nouvel indice de sécheresse pour les domaines méditerranéens. Application au bassin du Guadalquivir (sudouest de l'Espagne). *Publ. I Assoc. Int. Clim.* **2001**, *13*, 225–233.
34. McKee, T.B.; Doesken, N.J.; Kleist, J. The relationship of drought frequency and duration to time scales. In Proceedings of the Eighth Conference on Applied Climatology, Anaheim, CA, USA, 17–22 January 1993; p. 6.
35. Gong, X.; Richman, M.B. On the application of cluster analysis to growing season precipitation data in North America east of the Rockies. *J. Clim.* **1995**, *8*, 897–931. [CrossRef]
36. Santos, J.F.; Pulido-Calvo, I.; Portela, M.M. Spatial and temporal variability of droughts in Portugal. *Water Resour. Res.* **2010**, *46*, W03503. [CrossRef]
37. World Meteorological Organization—WMO. *Standardized Precipitation Index—User Guide*; World Meteorological Organization—WMO: Geneva, Switzerland, 2012; Volume WMO-No. 1090, p. 24.
38. Physical Sciences Laboratory—PSL/NOAA. Climate Indices: Monthly Atmospheric and Ocean Time-Series. Available online: https://psl.noaa.gov/data/climateindices/list/ (accessed on 1 July 2021).
39. Climate Prediction Center—CPC/NCEP/NOAA. Global Ocean Monitoring: Recent Evolution, Current Status, and Predictions. Available online: http://www.cpc.ncep.noaa.gov/products/GODAS/ (accessed on 10 June 2021).
40. Forootan, E.; Khaki, M.; Schumacher, M.; Wulfmeyer, V.; Mehrnegar, N.; Dijk, A.I.J.M.V.; Brocca, L.; Farzaneh, S.; Akinluyi, F.; Ramillien, G.; et al. Understanding the global hydrological droughts of 2003–2016 and their relationships with teleconnections. *Sci. Total Environ.* **2019**, *650*, 2587–2604. [CrossRef]
41. Metsalu, T.; Vilo, J. ClustVis: A web tool for visualizing clustering of multivariate data using Principal Component Analysis and heatmap. *Nucleic Acids Res. Adv. Access* **2015**, *43*, W566–W570. [CrossRef]
42. Intergovernmental Panel on Climate Change—IPCC. *Managing the Risks of Extreme Events and Disasters to Advance Climate Change Adaptation*; Cambridge University Press: Cambridge, UK; New York, NY, USA, 2012; p. 582.
43. Frölicher, T.L.; Fischer, E.M.; Gruber, N. Marine heatwaves under global warming. *Nature* **2018**, *560*, 360–364. [CrossRef]
44. Hobday, A.J.; Alexander, L.V.; Perkins, S.E.; Smale, D.A.; Straub, S.C.; Oliver, E.C.J.; Benthuysen, J.; Burrows, M.T.; Donat, M.G.; Feng, M.; et al. A hierarchical approach to defining marine heatwaves. *Prog. Oceanogr.* **2015**, *141*, 227–238. [CrossRef]
45. Eakin, C.M.; Morgan, J.A.; Heron, S.F.; Smith, T.B.; Liu, G.; Alvarez-Filip, L.; Baca, B.; Bartels, E.; Bastidas, C.; Bouchon, C.; et al. Caribbean corals in crisis: Record thermal stress, bleaching, and mortality in 2005. *PLoS ONE* **2010**, *5*, e13969. [CrossRef]
46. Gawarkiewicz, G.; Chen, K.; Forsyth, J.; Bahr, F.; Mercer, A.M.; Ellertson, A.; Fratantoni, P.; Seim, H.; Haines, S.; Han, L. Characteristics of an Advective Marine Heatwave in the Middle Atlantic Bight in Early 2017. *Front. Mar. Sci.* **2019**, *6*, 712. [CrossRef]
47. Bond, N.A.; Cronin, M.F.; Freeland, H.; Mantua, N. Causes and impacts of the 2014 warm anomaly in the NE Pacific. *Geophys. Res. Lett.* **2015**, *42*, 3414–3420. [CrossRef]
48. Amaya, D.J.; Miller, A.J.; Xie, S.-P.; Kosaka, Y. Physical drivers of the summer 2019 North Pacific marine heatwave. *Nat. Commun.* **2020**, *11*, 1903. [CrossRef]
49. Fewings, M.R.; Brown, K.S. Regional Structure in the Marine Heat Wave of Summer 2015 Off the Western United States. *Front. Mar. Sci.* **2019**, *6*, 564. [CrossRef]
50. Arafeh-Dalmau, N.; Montaño-Moctezuma, G.; Martínez, J.A.; Beas-Luna, R.; Schoeman, D.S.; Torres-Moye, G. Extreme Marine Heatwaves Alter Kelp Forest Community Near Its Equatorward Distribution Limit. *Front. Mar. Sci.* **2019**, *6*, 499. [CrossRef]
51. Laufkötter, C.; Zscheischler, J.; Frölicher, T.L. High-impact marine heatwaves attributable to human-induced global warming. *Science* **2020**, *369*, 1621–1625. [CrossRef]
52. Holbrook, N.J.; Scannell, H.A.; Gupta, A.S.; Benthuysen, J.A.; Feng, M.; Oliver, E.C.J.; Alexander, L.V.; Burrows, M.T.; Donat, M.G.; Hobday, A.J.; et al. A global assessment of marine heatwaves and their drivers. *Nat. Commun.* **2019**, *10*, 2624. [CrossRef]
53. Hartmann, D.L. Pacific sea surface temperature and the winter of 2014. *Geophys. Res. Lett.* **2015**, *42*, 1894–1902. [CrossRef]
54. Joh, Y.; Di Lorenzo, E. Increasing Coupling Between NPGO and PDO Leads to Prolonged Marine Heatwaves in the Northeast Pacific. *Geophys. Res. Lett.* **2017**, *44*, 11663–11671. [CrossRef]
55. Batista Silva, C.B.; Siqueira Silva, M.E.; Ambrizzi, T. Climatic variability of river outflow in the Pantanal region and the influence of sea surface temperature. *Theor. Appl. Climatol.* **2016**, *129*, 97–109. [CrossRef]
56. Rodrigues, R.R.; Taschetto, A.S.; Gupta, A.S.; Foltz, G.R. Common cause for severe droughts in South America and marine heatwaves in the South Atlantic. *Nature Geosci.* **2019**, *12*, 620–626. [CrossRef]
57. Rodrigues, R.R.; Taschetto, A.S.; Gupta, A.S.; Foltz, G.R. From severe droughts in South America to marine heatwaves in the South Atlantic. *EGU Gen. Assem.* **2020**, 5162. [CrossRef]

58. Parris, T.M. *Global Water Monitor & Forecast Watch List*; ISciences, L.L.C.: Burlington, VT, USA, 2021.
59. Damasceno, G.A., Jr.; de Roque, F.O.; Garcia, L.C.; Bandini Ribeiro, D.W.M.T.; Scremin-Dias, E.; Dias, F.A.; Libonati, R.; Rodrigues, J.A.; Lemos, F.; Santos, M.; et al. Lessons to be Learned from the Wildfire Catastrophe of 2020 in the Pantanal Wetland. *Wetl. Sci. Pract.* **2021**, *38*, 107–115.
60. Jacox, M.G. Marine heatwaves in a changing climate. *Nature* **2019**, *571*, 485–487. [CrossRef]
61. Song, Y.; Zhao, Y.; Yin, X.; Bao, Y.; Qiao, F. Evaluation of FIO-ESM v1.0 Seasonal Prediction Skills Over the North Pacific. *Front. Mar. Sci.* **2020**, *7*, 504. [CrossRef]
62. Von Schuckmann, K.; Traon, P.-Y.L.; Smith, N.; Pascual, A.; Djavidnia, S.; Gattuso, J.-P.; Grégoire, M.; Nolan, G.; Aaboe, S.; Fanjul, E.Á.; et al. Copernicus Marine Service Ocean State Report, Issue 4. *J. Oper. Oceanogr.* **2020**, *13*, S1–S172. [CrossRef]
63. Intergovernmental Panel on Climate Change—IPCC. *Climate Change 2013: The Physical Science Basis. Contribution of Working Group I to the Fifth Assessment Report of the Intergovernmental Panel on Climate Change*; Cambridge University Press: Cambridge, UK; New York, NY, USA, 2013; p. 1535.
64. Intergovernmental Panel on Climate Change—IPCC. *IPCC Special Report on the Ocean and Cryosphere in a Changing Climate*; Pörtner, H.-O., Roberts, D.C., Masson-Delmotte, V., Zhai, P., Tignor, M., Poloczanska, E., Mintenbeck, K., Alegría, A., Nicolai, M., Okem, A., et al., Eds.; in press. Available online: https://www.ipcc.ch/srocc/ (accessed on 10 October 2021).
65. Cheng, L.; Abraham, J.; Zhu, J.; Trenberth, K.E.; Fasullo, J.; Boyer, T.; Locarnini, R.; Zhang, B.; Yu, F.; Wan, L.; et al. Record-Setting Ocean Warmth Continued in 2019. *Adv. Atmos. Sci.* **2020**, *37*, 137–142. [CrossRef]
66. Scannell, H.A.; Johnson, G.C.; Thompson, L.; Lyman, J.M.; Riser, S.C. Subsurface Evolution and Persistence of Marine Heatwaves in the Northeast Pacific. *Geophys. Res. Lett.* **2020**, *47*, e2020GL090548. [CrossRef]
67. Li, G.C.; Cheng, L.J.; Zhu, J.; Trenberth, K.E.; Mann, M.E.; Abraham, J.P. Increasing ocean stratification over the past half century. *Nat. Clim. Chang.* **2020**, *10*, 1116–1123. [CrossRef]
68. Cheng, L.; Abraham, J.; Trenberth, K.E.; Fasullo, J.; Boyer, T.; Locarnini, R.; Zhang, B.; Yu, F.; Wan, L.; Chen, X.; et al. Upper Ocean Temperatures Hit Record High in 2020. *Adv. Atmos. Sci.* **2021**, *38*, 523–530. [CrossRef]
69. World Meteorological Organization—WMO. *State of the Global Climate 2020a*; WMO-No. 1264; World Meteorological Organization: Geneva, Switzerland, 2021; p. 56.
70. Cheng, L.J.; Abraham, J.; Hausfather, Z.; Trenberth, K.E. How fast are the oceans warming? *Science* **2019**, *363*, 128–129. [CrossRef]